Bioorganic Chemistry 114 (2021) 105139

Contents lists available at ScienceDirect

Bioorganic Chemistry

journal homepage: www.elsevier.com/locate/bioorg

In quest of small-molecules as potent non-competitive inhibitors against influenza

Khushboo Malbari [a], Priyanka Saha [b], Mamta Chawla-Sarkar [b], Shanta Dutta [b], Swita Rai [a], Mamata Joshi [c], Meena Kanyalkar [a,*]

[a] Department of Pharmaceutical Chemistry, Prin K M Kundnani College of Pharmacy, Cuffe Parade, Mumbai 400005, India
[b] Division of Virology, ICMR-National Institute of Cholera and Enteric Diseases (ICMR-NICED), Beleghata, Kolkata 700010, India
[c] National Facility for High Field NMR, Tata Institute of Fundamental Research (TIFR), Colaba, Mumbai 400005, India

ARTICLE INFO

Keywords:
430-cavity
Neuraminidase
Non-competitive inhibition
Pandemic H1N1
Influenza

ABSTRACT

A series of scaffolds namely aurones, 3-indolinones, 4-quinolones and cinnamic acid-piperazine hybrids, was designed, synthesized and investigated *in vitro* against influenza A/H1N1pdm09 virus. Designed molecules adopted different binding mode i.e., in 430-cavity of neuraminidase, unlike sialic acid and oseltamivir in molecular docking studies. All molecules reduced the viral titer and exhibited non-cytotoxicity along with cryoprotective property towards MDCK cells. Molecules (*Z*)-2-(3′-Chloro-benzylidene)-1,2-dihydro-indol-3-one (**2f**), (*Z*)-2-(4′-Chloro-benzylidene)-1,2-dihydro-indol-3-one (**2g**) and 2-(2′-Methoxy-phenyl)-1H-quinolin-4-one (**3a**) were the most interesting molecules identified in this research, endowed with robust potencies showing low-nanomolar EC_{50} values of 4.0 nM, 6.7 nM and 4.9 nM, respectively, compared to reference competitive and non-competitive inhibitors: oseltamivir (EC_{50} = 12.7 nM) and quercetin (EC_{50} = 0.56 μM), respectively. Besides, **2f, 2g** and **3a** exhibited good neuraminidase inhibitory activity in sub-micromolar range (IC_{50} = 0.52 μM, 3.5 μM, 1.3 μM respectively). Moreover, these molecules were determined as non-competitive inhibitors similar to reference non-competitive inhibitor quercetin unlike reference competitive inhibitor oseltamivir in kinetics studies.

1. Introduction

Influenza A/H1N1pdm09, despite being a mild pandemic, remains a critical challenge to public health in terms of mortality and morbidity. In addition, one cannot rule out further inter genotypic reassortment events with currently circulating high pathogenic avian influenza strains such as H5N1 and H9N2 [1–3]. The influenza life cycle depends on an accurate balance between the functionality of two viral surface glycoproteins *viz.* Hemagglutinin (HA) and Neuraminidase (NA). HA being a fusion protein, facilitates the fusion of endocytosed virus particle with the host cell endosomal membrane after binding to the surface receptors containing sialic acid (SA). This brings about the viral internalization. NA being an exosialidase, cleaves the α-ketosidic linkage between SA and adjacent sugar residue [4,5]. The virulence and replication of a pandemic H1N1 strain has been reported to be greater than that for a seasonal H1N1 strain, and this difference increases the severity of the disease [6,7].

The anti-influenza drugs currently used as treatment, such as oseltamivir (OMV) and zanamivir (ZMV), have the structural similarity to SA and consequently similar binding pattern to the NA enzyme. But, mutations in NA gene limits their use as competitive inhibitors due to resistance [8,9]. This reinforces the requirement of an alternate approach in design and synthesis of new molecules to be developed as potential anti-influenza agents. This could be achieved by discovery of newer scaffolds that are structurally dissimilar to OMV/ZMV and have different binding pattern in the enzyme cavity. The resistance problem

Abbreviations: CAPi, Cinnamic acid-piperazine; CC, Cell control; CV, Crystal violet; CPE, Cytopathic effect; DCM, Dichloromethane; DMF, Dimethyl formamide; DMSO, Dimethylsulfoxide; FBS, Foetal Bovine Serum; HA, Hemagglutinin; HA titer, Hemagglutination titer; HAI, Hemagglutination inhibition; LR, Laboratory Reagent; MDCK, Madin-Darby Canine Kidney cells; MEM, Minimum Essential Medium; NA, Neuraminidase; OMVC, Oseltamivir Carboxylate; OMVP, Oseltamivir Phosphate; PDB, Protein Data Bank; QR, Quercetin; SA, Sialic Acid; VC, VirusControl.

* Corresponding author at: Department of Pharmaceutical Chemistry, Prin. K. M. Kundnani College of Pharmacy, Plot 23, Jote Joy Building, Rambhau Salgaonkar Marg, Cuffe Parade, Mumbai 400005, India.
E-mail address: ma.kanyalkar@kmkcp.edu.in (M. Kanyalkar).

https://doi.org/10.1016/j.bioorg.2021.105139
Received 18 November 2020; Received in revised form 14 May 2021; Accepted 28 June 2021
Available online 1 July 2021

towards competitive inhibitors of NA i.e., OMV and ZMV, due to mutations could be avoided by developing non-competitive inhibitors which inhibit the enzyme by binding allosterically to the target enzyme. There are two cavities present adjacent to SA/OMV binding site in NA *viz.*, 150-cavity and 430-cavity. These two cavities could be considered as the potential alternate binding sites in NA.

There are reported molecules that bind to 150-cavity and 430-cavity demonstrating potent inhibition of various NA subtypes [10,11]. In fact, in recent years, discovery of various molecules, by our lab team, probing 150-cavity and 430-cavity led us to a series of chalcones showing non-competitive inhibition mechanism towards H1N1-NA and H5N1-NA along with certain other scaffolds, showing anti-influenza activities against H1N1-NA [12–15]. Among several reported antiviral phyto-constituents and our lab team's findings, we have selected chalcones that is characterized by α, β-unsaturated carbonyl functional groups. Nonetheless, chalcones show weaker anti-influenza activity along with cytotoxicity [16–19]. This scaffold can be modified to various cyclized derivatives such as aurones, flavones, 3-indolinones and 4-quinolones, for cyclized rigidification has been proven to improve the activity of a lead molecule [20]. Chalcones, the chosen parent scaffold, can correspondingly be compared with other α, β-unsaturated carbonyl functional group containing phytoconstituent showing antiviral activity such as cinnamic acid derivatives [21–23]. Further, piperazine moiety, having wide variety of activity [24,25], is a commonly used scaffold in various drugs, and thus had been selected and linked with cinnamic acid scaffold by molecular hybridization approach [26]. Therefore, considering the above facts and modifications, we report here the design, synthesis and evaluation of a series of four scaffolds, namely aurones, 3-indolinones, 4-quinolones and cinnamic acid-piperazine (CAPi) hybrids against influenza A/H1N1pdm09 virus. The above-mentioned selected scaffolds are structurally dissimilar to the transition state of sialo-glycoconjugate being hydrolysed by viral NA, the substrate for NA. They were designed with introducing substituents with varied functional groups attributing electronic, steric and volume effect to the molecules.

Cytopathic effect (CPE) inhibition and hemagglutination inhibition (HAI) assays were executed on the molecules that were selected based on docking results and cytotoxicity, to screen them for further extensive evaluation studies on the basis of % CPE inhibition and % HA titer reduction of virus with candidate molecules. All the screened molecules were subjected to cell-based assay to determine their EC_{50} values followed by enzyme-based assay to determine their IC_{50} values. Additionally, mechanism of inhibition of the molecules was determined by enzyme kinetics studies which showed non-competitive inhibition when compared with competitive inhibitor *viz.* OMV. This strengthens our idea of developing potential anti-influenza agents and propose better therapeutic and prophylactic upshots than what current anti-influenza drugs can offer us.

Also, there has been studies conducted to suggest the corelation between influenza and SARS-CoV-2 [27]. It was demonstrated that influenza caused increase in the SARS-CoV-2 transmission along with enabling the spread of COVID-19 in Europe during early 2020. More generally, taking into account the resistance issue of influenza, it is imperative to develop agents with alternate mechanism of action that this current work is all about that can combat this very contributing factor of influenza to the spread of COVID-19.

2. Results and discussion

2.1. Computational studies demonstrating alternate binding mode in NA enzyme

The active site of N1-NA was classified into three cavities for suitability: (i) the SA catalytic cavity (R118, E119, N146, D151, R152, Y178, I222, E227, E276, E277, R292, N294, N347, R371, and Y406); (ii) the 150-cavity (N146-R152) and (iii) the 430-cavity (N325, P326, G348, S369, S370, W403, I427, G429, R430-T439) [13,28]. Interestingly, the crystal structure of NA from the pandemic 2009 influenza A/H1N1pdm09 strain indicated that it lacks the 150-loop in its active site (akin to closed conformation in contrast to the open conformation observed in seasonal H1N1-NA influenza attributed to the presence of 150-loop) [29–33]. The initial docking validation studies could acceptably replicate (RMSD 0.32 Å) the binding pose of the co-crystallized ligand *viz.* oseltamivir carboxylate (OMVC) in the influenza A/H1N1pdm09-NA X-ray crystal structure (PDB ID: 3TI6). The cleavage of α-ketosidic linkages between SA and adjacent sugar residue occurs during NA catalyses [8,34]. Thus, to understand the interaction pattern and critical residues involved in SA binding, we docked sialic acid in SA catalytic cavity of NA (Fig. 1**a**). It was observed that the carbonyl of *N*-acetamido group formed H-bond with R152 while the deoxy formed H-bond with E277. The terminal hydroxyl groups of glycerol sidechain formed H-bond with R118, E119, and Y406. The carboxylate group formed H-bond with the sidechain of R292 along with a bi-dentate interaction with R371. The hydroxyl group formed H-bond with R151.

To ensure about the unbiased search of binding site of our designed molecules, we explored all the putative binding pockets for docking in NA enzyme. This strategy is often applied when prior knowledge of the binding mode of the molecule is unknown [35,36]. Initially, we docked quercetin, active natural non-competitive anti-influenza agent [37] in NA to gain insight into its non-competitive inhibition behaviour. As anticipated from its non-competitive nature, quercetin did not bind to SA cavity, rather its binding was confined to 430-cavity within the active site than other putative binding pockets. Moreover, to ensure whether quercetin occupy distinctly different region than SA binding site or not, we have docked it into the active site of NA already complexed with OMVC/SA. It was observed that it still bound the same way as observed in absence of OMVC/SA. This confirmed that quercetin occupied a very distinct site and did not overlap with the SA binding site that further signified existence of an alternate binding region for quercetin within the catalytic site discrete from available drugs and SA (Fig. 1**b**). The two hydroxyl groups of flavone ring of quercetin formed H-bond with N347 and K432 along with π-alkyl interaction with R371 and P431. The hydroxyl of phenyl ring formed H-bond with I427 and phenyl ring had π-alkyl interaction with R371, I427, P431 and K432.

Additionally, non-bonded interaction energies were calculated for quercetin with the catalytic site residues. Fig. 2 demonstrates that quercetin has favourable non-bonded interactions with the catalytic site residues that included R118, I149, R152, N294, N347, S370, R371, W403, Y406, R430, P431, L432, T436, I437 and W438. The previously reported site-directed mutagenesis studies highlighted the importance of N146, R152, W178, E276, E277, S370, R371, W403, Y406 in the catalytic activity of NA [9,38], out of which quercetin showed non-bonded interactions with R152, S370, R371, W403 and Y406. Moreover, it was observed that R152 is involved in the binding of SA to active site of NA (*vide supra*) in molecular docking studies. Therefore, it could be presumed from the above outcomes that on account of H-bonding and non-bonded interactions, quercetin cause hinderance in the catalytic activity of NA thereby inhibiting it, nonetheless, with an alternate binding mode in the NA enzyme.

The designed molecules were then docked in influenza A/H1N1pdm09-NA enzyme to have knowledge of how substituting various functional groups at different positions and having the scaffold changed affect their binding mode in NA enzyme. The introduction of substituents may improve the pharmacokinetic and pharmacodynamic properties of the molecule by virtue of imparting electronic and lipophilic characters [39].

The comprehensive analysis of molecular docking studies highlighted that the binding affinity of our designed molecules was confined to the 430–cavity similar to quercetin, which was considered as the standard for non-competitive inhibition, unlike SA and OMVC as shown in Fig. 3. In the series of aurones, the benzofuranone ring of all molecules occupied the hydrophobic cavity (W403, I427, P431, K432). Molecules

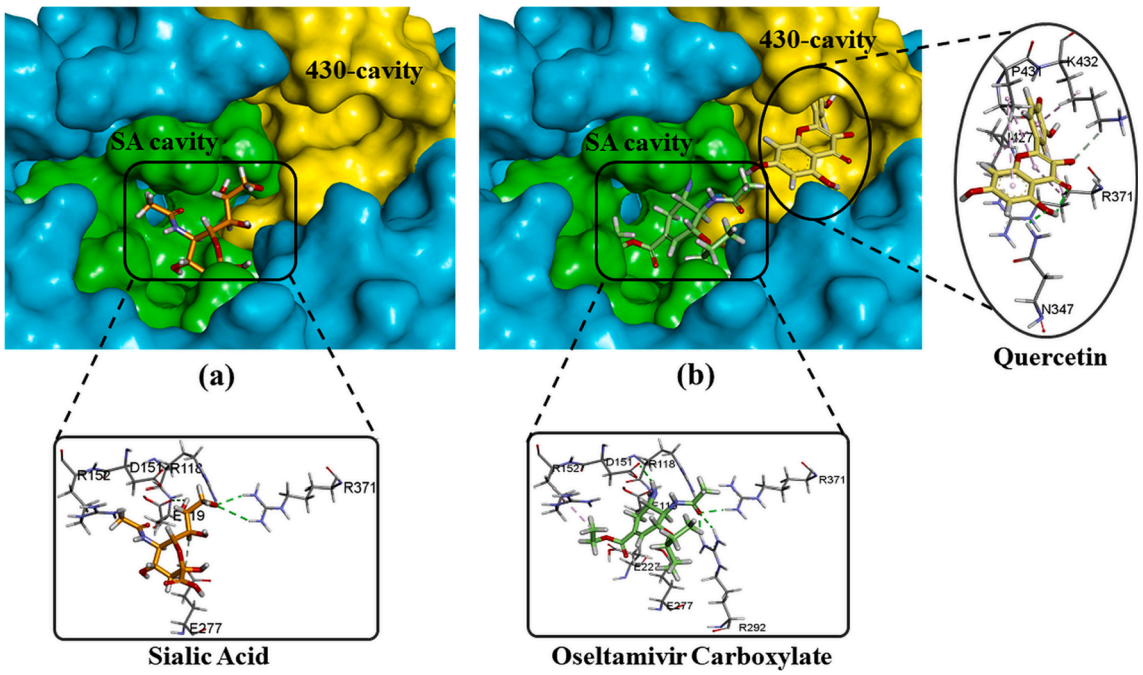

Fig.1. Docked poses of (a) sialic acid (orange colour) in SA cavity and (b) oseltamivir carboxylate (green colour) in SA cavity and quercetin (yellow colour) in 430-cavity of H1N1-NA enzyme. The SA cavity is represented in green colour and 430-cavity is represented in yellow colour in the surface model. The figure was prepared using Discovery Studio visualizer tool. (For interpretation of the references to colour in this figure legend, the reader is referred to the web version of this article.)

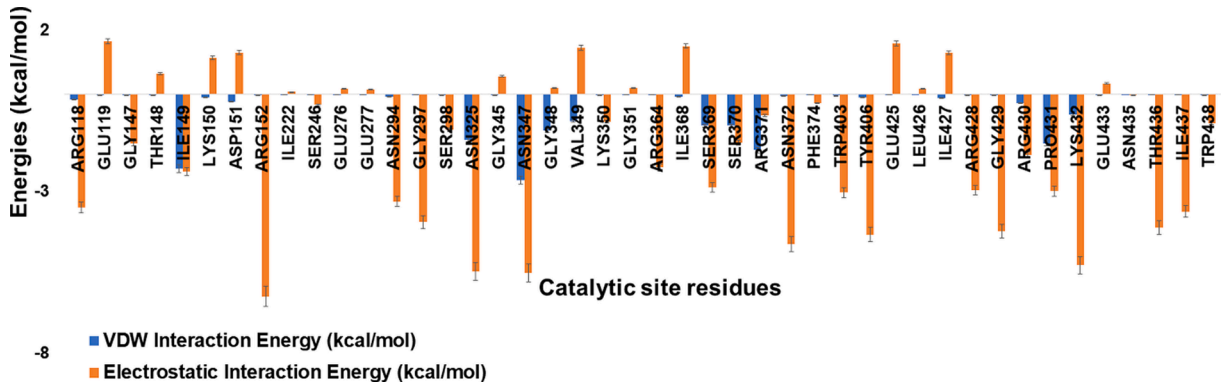

Fig.2. Histogram of interaction energies (van der Waal i.e., vdW and Electrostatic) of quercetin with the catalytic site residues.

1a-1c showed H-binding with K432. **1d** showed H-bond interactions with R371 and N347; while **1e** had electrostatic interaction with W403 and salt bridge with D283. The docked conformations of 3-indolinone molecules **2a-2e, 2g** and **2h** revealed that the 3-indolinone ring of these molecules had hydrophobic interactions with I427, P431 and K432 along with hydrogen bond and hydrophobic interactions with R371; while the phenyl ring interacted hydrophobically with P326. However, molecule **2f** had reverse orientation in which the phenyl ring showed hydrophobic interactions with I427, P431 and K432 along with interaction of its *m*-chloro group with R371 and W403; while the 3-indolinone ring had hydrogen bond and hydrophobic interaction with R371, which could be responsible for its higher activity. The molecules **3a**, **3c-3f, 3h** and **3i** were docked such that commonly the 4-quinolone ring of these molecules had hydrophobic interactions with R371, I427, P431 and K432 along with hydrogen bond and hydrophobic interaction with R371; while phenyl ring showed interaction with N347. **3b** and **3g** were docked in a different orientation than others having their phenyl ring interacting hydrophobically with I427, P431 and K432 and with R371 as well showing hydrogen bond and hydrophobic interaction; while the 4-quinolone ring showed hydrogen bond interactions with R118 and I149. The molecules **4a-4e** were docked with their phenyl ring interacting hydrophobically with I427, P431 and K432 along with hydrogen bond and hydrophobic interaction with R371. The piperazine ring of CAPi hybrid molecules had hydrogen bond interactions with N347 and S369. It is evident that additionally, all the designed molecules have either H-bonding or hydrophobic interaction with backbone and sidechain of R371. Detailed analysis of binding interactions of the molecules with NA enzyme is depicted in Table 1.

The observations from computational studies recommended that the molecules might bind tight to the NA enzyme attributed to their additional interactions, consequently leading to better anti-influenza activity.

The pharmacological activity and the performance of a drug candidate can be predicted to some extent by determining their ADME properties. Accurate prediction of *in vivo* pharmacological activity of a potential drug molecule is the ultimate aim of *in-silico* ADME studies [40]. Various descriptors were evaluated for ADME properties of candidate molecules. None of the designed molecules violated Lipinski's rule of five indicating towards their drug-likeness. All the molecules' molecular weight was in the range values of 130–725, donor HB

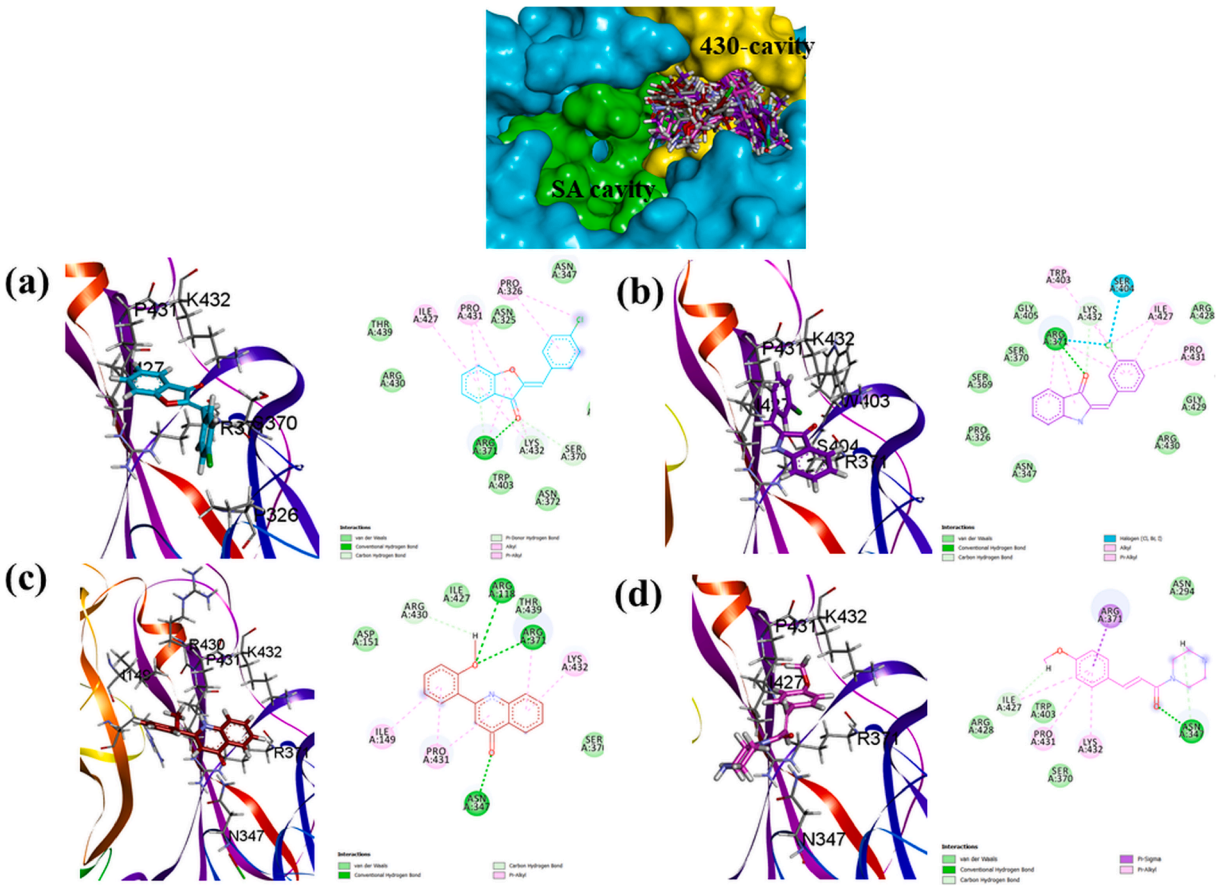

Fig.3. Docked poses of designed molecules in 430-cavity (top) in surface model of H1N1-NA enzyme. 3D docking model and corresponding 2D schematic diagram of docking model of representative (a) aurone, (b) 3-indolinone, (c) 4-quinolone and (d) cinnamic acid-piperazine hybrid.

(hydrogen bond) and acceptor HB were in the range of 0–6 and 2–20 respectively. Solvent accessible surface area (SASA) is an indication of the partition coefficient and aqueous solubility which was found to be in the range of 300–1000 for all the deigned molecules [41]. The bioavailability of a molecule is considerably determined by QPlogPo/w which was found to be favourable in the range of −2 to 6.5. The ionization potential parameter is indicative of distribution of molecule that affects the molecule's availability for further physical, chemical or biological reactions. The solute ionization potential (eV) was found to be in the range of 7.9–10.5 for all the molecules. It is indicated that the designed molecules possess favourable pharmacokinetic properties evident from the overall *in-silico* ADME results.

2.2. Chemistry

Based on the outcomes of computational studies of newly designed four scaffolds; with respect to their interactions with the enzyme, their binding poses and affinity; twenty-seven molecules corresponding to four scaffolds were synthesized *viz.* five aurones (**1a-1e**), eight 3-indolinones (**2a-2h**), nine 4-quinolones (**3a-3i**), and five CAPi hybrids (**4a-4e**). The target molecules were synthesized as shown in Scheme 1 and Scheme 2. The IR spectra demonstrated expected absorption bands for the functional groups of the synthesized molecules. All the aurone molecules showed cyclic C—O stretching near 1300 cm^{-1}. The absorption band for NH stretching in 3-indolinone molecules was observed near 3450–3100 cm^{-1}, while that for 4-quinolones was observed near 3232–3080 cm^{-1} and that for CAPi hybrids was observed near 3130 cm^{-1}. The IR band for carbonyl C═O stretch in aurones and 3-indolinones was around 1650 cm^{-1}, while that in 4-quinolones was around 1715 cm^{-1}. Carbonyl C═O stretch for CAPi hybrids was observed near 1640–1645 cm^{-1}. The exocyclic C═C in aurones and 3-indolinones was characterized by a band near 1660–1667 cm^{-1}, whereas the endocyclic C═C in 4-quinolones was near 1600–1620 cm^{-1}. The C═C stretch in CAPi hybrids was around 1600–1615 cm^{-1}. ^{1}H and ^{13}C NMR spectra of molecules represented predictable delta values for all aliphatic and aromatic protons and carbons, respectively. In ^{1}H NMR spectra of synthesized molecules, the vinylic proton of aurones and 3-indolinones (H-10) appeared in the range of δ 6.90–7.11 and δ 6.63–7.20, respectively as singlet, while the pyridone ring proton (H-3) in 4-quinolones showed chemical shift value in the range of δ 6.02–7.28 as singlet. The downfield appearance of vinylic proton (H-10) of 3-indolinones is the characteristics of *Z* isomer. We interpret this to be due to the H-10 proton being deshielded by the neighbouring carbonyl at C-3 position [42–45]. The NH of 3-indolinones and 4-quinolones appeared downfield around δ 10–12, while the piperazine NH appeared around δ 1.5–1.6. The chemical shift value of vinylic carbon (C-10) of aurones were in the range of δ 108.38–113.76 [46] represented in ^{13}C NMR which is the characteristics of thermodynamically more stable *Z* isomer. Mass spectra of representative synthesized molecules gave the predicted *m/z* peak corresponding to their estimated molecular weight. The HPLC purity of molecules was > 95%. Therefore, it was confirmed that the anticipated structures of the synthesized molecules are correct and are pure (Spectra in Supplementary data).

2.3. Anti-influenza evaluation

Oseltamivir phosphate (**OMVP**) was considered as standard for cellular assays, *viz.* MTT, CPE, HAI and CV assays, as the esterase enzyme present in cells convert it to its active metabolite i.e., oseltamivir carboxylate (**OMVC**) [47,48], while oseltamivir carboxylate was

Table 1
Detailed analysis of binding interactions of docked molecules with amino acid residues of H1N1-NA.

Residues		R118*	E119*	I149	D151*	R152*	R224*	R292*	P326	N347	S369	S370	R371*	W403	I427	R430	P431	K432	E433
Molecules	**1a**	H	–	–	–	–	–	–	–	H	–	–	H	–	–	–	–	H, π-a	–
	1b	–	–	–	–	–	–	–	–	H	–	–	H	–	–	–	–	H	–
	1c	H	–	–	–	–	–	–	–	H	–	–	H	π-π	–	–	–	H	–
	1d	–	–	–	–	–	–	–	π-a (2)	H	–	–	H (2), π-a	–	π-a	–	π-a (2)	H, π-a (2)	–
	1e	–	–	–	–	–	–	–	–	H	–	–	H	π-a, π-π	–	–	–	H	–
	2a	H (2)	–	–	–	–	–	–	H (2), π-a	H	–	H	H, π-a (2)	–	π-a	–	π-a (2)	π-a (2)	–
	2b	–	–	–	–	–	–	–	π-a	–	H	–	H, π-a, π-σ	–	π-a	–	π-a (2)	π-a (2)	–
	2c	–	–	–	–	–	–	–	π-a	–	–	H	H, π-a, π-σ	–	π-a	–	π-a (2)	π-π, π-a (2)	–
	2d	–	–	–	–	–	–	–	–	–	–	–	π-a, π-σ	–	π-a	–	π-a (3)	π-a (2)	–
	2e	–	–	–	–	–	–	–	π-a (2)	–	–	H	H, π-a, π-σ (2)	–	π-a	–	π-a (2)	π-a (2)	–
	2f	–	–	–	–	–	–	–	–	–	–	–	H, π-a (3), halogen	π-a	π-a (2)	–	π-a	H, π-a	–
	2g	–	–	–	–	–	–	–	π-a (2)	H	–	–	H, π-a, π-σ	–	π-a	–	π-a (2)	H, π-a (2)	–
	2h	–	–	–	–	–	–	–	π-a		–	H	H, π-a, π-σ	–	π-a	–	π-a (2)	π-a (2)	–
	3a	H	–	π-a	–	–	–	–	–	H	–	–	H, π-a	–	–	H	π-a (2)	π-a	–
	3b	H	–	–	–	–	–	–	–	–	–	H	H, π-a	–	π-a (2)	–	π-a (3)	H (2), π-a	–
	3c	–	–	–	–	–	–	–	–	H	–	H	H, π-a, π-σ	–	π-a	–	π-a (2)	H, π-a (2)	–
	3d	H	–	–	H	π-a	H, π-a	H	–		–		H	–	–	–	–	–	–
	3e	–	–	–	–	–	–	–	–	π-π	–	H	H, π-a, π-σ (2)	–	π-a	–	π-a (3)	H, π-a (2)	–
	3f	–	–	π-a	–	–	–	–	–	–	–	–	π-a	π-a	π-a (2)	H	π-a (2)	π-a (2)	–
	3g	H	–	π-a	–	–	–	–	–	–	–	–	π-a, π-σ	π-a	π-a	–	π-a (3)	H, π-a	–
	3h	–	–	–	–	–	–	H	–	H	–	H	H (2), π-a, π-σ	–	π-a	–	π-a (2)	H, π-a (2)	–
	3i	–	–	–	–	–	–	–	π-σ	H	–	–	H, π-a, π-σ	–	π-a (2)	–	π-a (2)	π-a (2)	–
	4a	–	–	–	–	–	–	–	–	–	–	H	H, π-σ	–	π-σ	–	π-σ	π-σ	–
	4b	–	–	–	–	–	–	–	–	H (2)	–	–	H, π-a	–	π-a	H	π-a	π-a	–
	4c	–	–	–	–	–	–	–	–	H (2)	–	–	π-σ	–	H, π-a	–	π-a	π-a	–
	4d	–	–	–	H	–	–	–	–	–	–	–	H, π-a, π-σ	H	H, π-a	–	π-a	π-a	–
	4e	–	–	–	–	–	–	–	–	–	H (2)	–	π-a	π-a	π-a	–	π-a	π-a (2)	Halogen

H: Hydrogen bond; π-π: pi- pi interaction (hydrophobic); π-a: pi-alkyl interaction (hydrophobic); π-σ: pi-sigma interaction (hydrophobic); *Catalytic site residues interacting with SA. Figures in brackets indicate number of bonds.

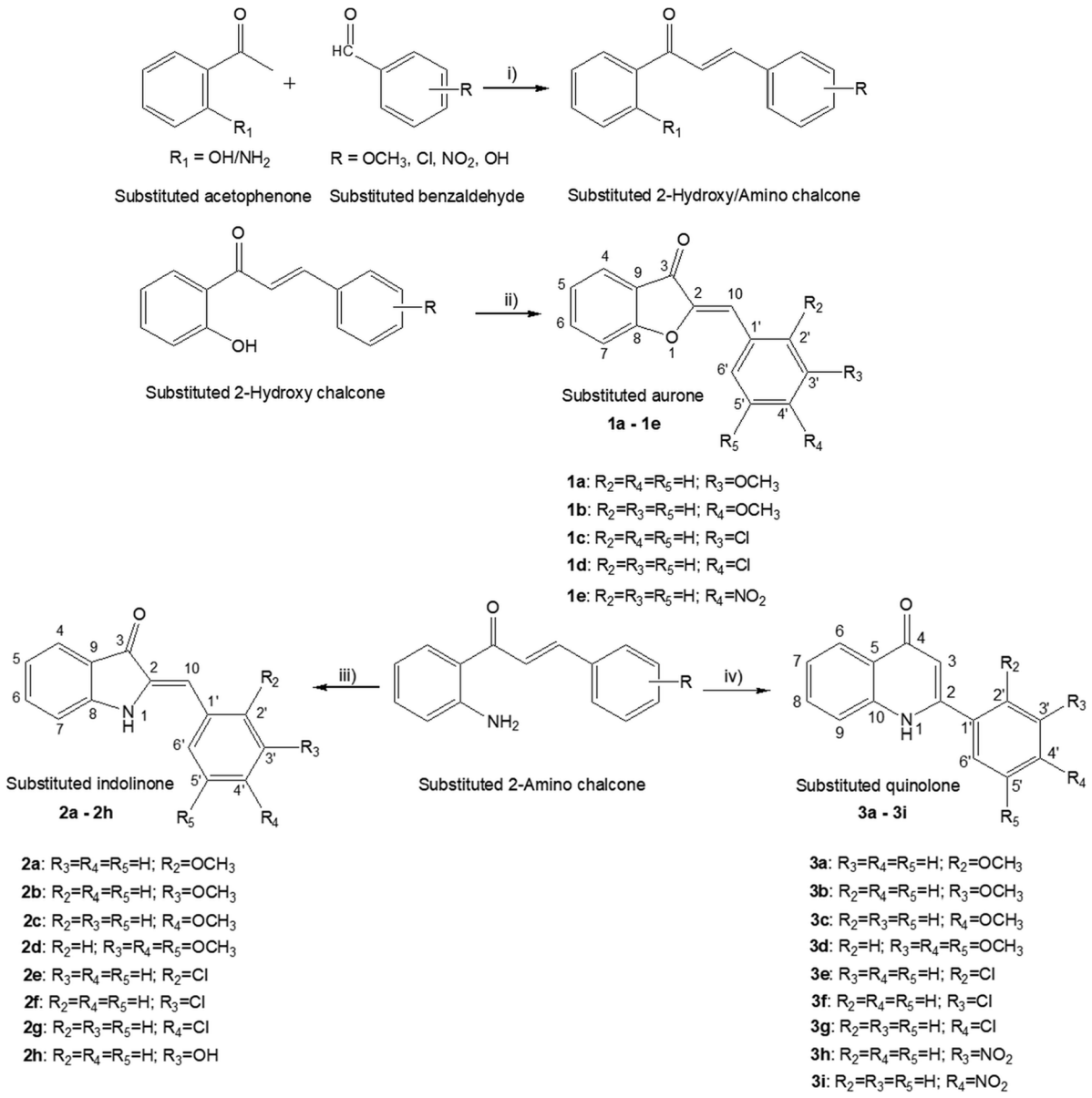

Scheme 1. Synthesis of aurone (**1a-1e**) from 2-hydroxychalcone; 3-indolinone (**2a-2h**) and 4-quinolone (**3a-3i**) from 2-aminochalcone. Reagents and conditions used: (i) 20% NaOH, absolute ethanol, 10 °C, 4–5 h; (ii) $Hg(OAC)_2$, pyridine, 110 °C, 1–2 h; (iii) acetic acid, 10% w/w Amberlyst-15, 80 °C, 2–5 h; (iv) DMSO, iodine crystal, reflux, 30 min.

directly used as standard for enzymatic assays *viz.* NA inhibition assay and enzyme kinetics studies. **OMVP**/**OMVC** and quercetin (**QR**, the reported natural non-competitive inhibitor[37]) were used as standards for representing the competitive and non-competitive inhibition, respectively.

2.3.1. Cytotoxicity studies of all the synthesized molecules

Cytotoxicity studies determined the concentration of synthesized molecules responsible for 50% reduction in cell viability (CC_{50}). The results of MTT-Formazan assay for cytotoxicity study of twenty-seven synthesized molecules indicated that they had no serious effect on MDCK cells except for molecule **4d** having CC_{50} of 40 μM (Table 2). The anti-influenza activity of these non-cytotoxic molecules was further evaluated for decrease in cytopathic effect (CPE) of influenza A/H1N1pdm09 strain in MDCK cells in presence of the molecules.

2.3.2. Cytopathic effect (CPE) inhibition of all the molecules

CPE inhibition assay of all twenty-seven synthesized molecules was carried out as qualitative evaluation study to assess the degree of viral inhibitory activity of the molecules after comparison with **OMVP** as standard drug. Interestingly, CPEs in the form of loss of cell adhesion that is the characteristics of influenza A/H1N1pdm09 virus infection were found to be considerably reduced in our synthesized molecule-treated infected cells, further asserting a robust cyto-protective and anti-influenza property of these molecules. The degree of inhibition of viral CPE by all the evaluated molecules is depicted in supplementary table, Table S1. All the molecules showed at least 50% CPE inhibition suggestive of the substantial ability of molecules to reduce the viral load. Subsequently, they were carried forward for further assays.

2.3.3. Hemagglutination inhibition (HAI) to determine viral titer reduction by molecules

The CPE inhibition was further assessed by comparing the HA titer of virus in virus control well with the HA titer of virus in molecule-treated wells. Relative viral load *viz.* the HA titer of molecule-treated infected cells was represented as '% HA titer reduction' considering the

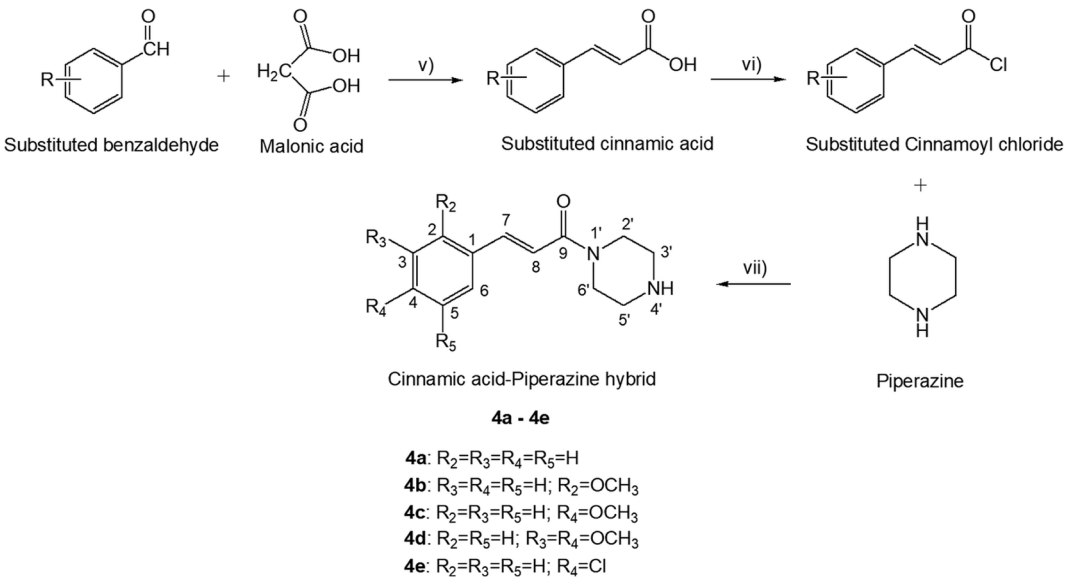

Scheme 2. Synthesis of cinnamic acid-piperazine hybrid (**4a-4e**). Reagents and conditions: (v) pyridine/piperidine, 100 °C, 2 h; (vi) DCM, thionyl chloride, DMF, reflux, 24 h; (vii) DCM, TEA, 0 °C till reaction completed monitored by TLC.

infectivity, in terms of HA titer, of the vehicle-treated infected control as 100% in each replicate of triplicate experiments. OMVP and QR were used as standards, and %HA viral titer reduction data for all the molecules are summarized in Table 3**.** As evident from data, most of the molecules caused robust and persistent reduction in the viral titer at least by 50%, as shown in Fig. 4. The results of HAI assay illustrated that our molecules efficiently suppress the viral titer showing weak-to-moderate-to-high potencies compared to standards (OMVP = 85 ± 4% and QR = 79 ± 4%, at 100 μM) further directing towards the anti-influenza activity of the molecules. The structure–activity relationship was tough to draw, attributed to the vague outline between these molecules and reduction rates of %HA titer. Next, the molecules were carried further for quantitative evaluation of their anti-influenza activity.

2.3.4. Cell-based crystal violet (CV) assay to quantify the effective concentration of molecules

CV assay determined quantitatively the effective concentration of tested molecules that resulted in 50% cell survival (EC_{50}). Consistent with the marked attenuated viral HA titer, the tested molecules notably showed significant degrees of cell survival in CV assay (Table 2). Molecules **2f** (3-indolinone with *m*-chloro group on benzyl ring), **2g** (3-indolinone with *p*-chloro group on benzyl ring) and **3a** (4-quinolone with *o*-methoxy group on phenyl ring) having EC_{50} of 4.0 ± 0.1 nM, 6.7 ± 0.1 nM and 4.9 ± 0.1 nM, respectively, had highest activity with their EC_{50} values better than commercial drug i.e., **OMVP** (EC_{50} = 12.7 ± 0.3 nM) as well as **QR** (EC_{50} = 0.56 ± 0.01 μM). Molecules **1d** (aurone with *p*-chloro group on benzyl ring) and **2b** (3-indolinone with *m*-methoxy group on benzyl ring) with EC_{50} = 39 ± 2 nM and 25 ± 1 nM, respectively, however were slightly less active than **OMVP,** but better than **QR**, still could be believed to have remarkable anti-influenza property. The effects of representative potent molecules along with standards on % cell survival infected with pdmH1N1 virus are shown in Fig. 5. These results suggested that these molecules could hamper overall replication of virus in MDCK cells. The high selectivity index values of these compounds indicated that they decreased the virus replication without adverse effect on the living host cells.

2.3.5. Enzyme-based NA inhibition to determine inhibitory concentration of molecules

H1N1-NA inhibition by twenty-five molecules, based on CV assay, was determined by calculating the concentration required to inhibit 50% of the enzyme activity (IC_{50}). Dose response curves depicting the effect of our molecules on H1N1-NA enzyme are shown in Fig. 6.

The IC_{50} values of the evaluated molecules ranged from 0.52 ± 0.01 μM to 24.6 ± 1.3 μM. **OMVC** and **QR**, the standards chosen in enzyme-based assay, has IC_{50} value of 1.9 ± 0.1 nM and 8.7 ± 0.1 μM, respectively (Table 2). Though the potent molecules discussed in CV assay had their IC_{50} values lower than **OMVC**, they certainly tend to exhibit excellent activity with their IC_{50} values at low-micromolar level, intriguingly, better than **QR**. The trend of efficacy of molecules seen in CV assay is followed in NA inhibition assay as well, the potent molecules **2f** (IC_{50} = 0.52 ± 0.01 μM)**, 2g** (IC_{50} = 3.5 ± 0.1 μM) and **3a** (IC_{50} = 1.3 ± 0.2 μM) possessed lowest IC_{50} values than other molecules of the series. Interestingly, the combined results of CV assay and NA inhibition studies suggested that the evaluated molecules suppress overall viral replication than inhibiting the NA enzyme *per se*. These results pointed towards the fact that there might be an accompanying mechanism by which our evaluated molecules control virus replication indicated by their potency *in vitro*.

2.3.6. Enzyme kinetics studies to ascertain mechanism of inhibition of molecules

Enzyme kinetics study was performed on eleven most active molecules (based on CV and NA inhibition assay) to validate the non-competitive inhibition of designed molecules as exhibited by docking studies. In this study, **OMVC** and **QR** were used as standards for competitive and non-competitive inhibition, respectively. Unsurprisingly, **OMVC** being structurally similar and transition state analogue of SA, showed competitive inhibition evident from the plots exhibited in Fig. 7 which shows Lineweaver-Burk plot of 1/V versus 1/[S]. The plots were obtained by considering absence of inhibitor molecule (i.e., at 0 nM concentration) and at two concentrations bracketing the IC_{50} value of the inhibitor molecule. Increasing concentrations of **OMVC** (K_i = 2.8 × 10^{-4} μM) resulted in collection of lines with increased K_m while the V_{max} remained unaffected i.e., they have equivalent y-axis intercept but with higher value of x-axis intercept. This indicated its competitive inhibition. However, increasing concentrations of **QR** (K_i = 5.1 μM) resulted in collections of lines wherein the K_m remained unaffected while V_{max} showed reduction i.e., they have equivalent x-axis intercepts along with increase in the y-axis intercept values. This demonstrated its anticipated non-competitive inhibition as reported in literature.

Interestingly, in case of our evaluated molecules, the Lineweaver-

Table 2
In-vitro evaluation of tested molecules.

Sr. No.	Molecules	CC_{50} (μM)	EC_{50} (μM)	SI	IC_{50} (μM)	Ki (μM)
1	**1a**	193 ± 1	>100	–	Not tested	Not tested
2	**1b**	171 ± 1	1.5 ± 0.9	117	9.3 ± 0.1	10.5 ± 0.7
3	**1c**	120 ± 1	1.0 ± 0.1	118	14.9 ± 1.2	Not tested
4	**1d**	113 ± 1	(39 ± 2) × 10^3	2.9 × 10^3	1.8 ± 0.1	11.2 ± 2.8
5	**1e**	111 ± 1	>100	–	Not tested	Not tested
6	**2a**	263 ± 1	5.1 ± 0.9	52	20.9 ± 1.3	Not tested
7	**2b**	292 ± 1	(25 ± 1) × 10^3	1.2 × 10^4	22.4 ± 1.3	2.6 ± 0.1
8	**2c**	287 ± 1	11.9 ± 1.3	24	10.5 ± 1.2	Not tested
9	**2d**	128 ± 1	0.17 ± 0.05	752	19.8 ± 1.3	Not tested
10	**2e**	269 ± 1	3.1 ± 0.1	88	19.4 ± 1.2	Not tested
11	**2f**	272 ± 1	(4.0 ± 0.1) × 10^3	6.8 × 10^4	0.52 ± 0.01	2.8 ± 0.2
12	**2g**	192 ± 1	(6.7 ± 0.1) × 10^3	2.8 × 10^4	3.5 ± 0.1	2.0 ± 0.003
13	**2h**	115 ± 1	0.25 ± 0.01	462	15.7 ± 1.2	33.7 ± 2.3
14	**3a**	286 ± 1	(4.9 ± 0.1) × 10^3	5.8 × 10^4	1.3 ± 0.2	2.1 ± 0.2
15	**3b**	235 ± 1	>100	–	24.3 ± 1.3	Not tested
16	**3c**	277 ± 1	>100	–	3.8 ± 0.1	53.6 ± 9
17	**3d**	200 ± 1	>100	–	12.2 ± 1	2.8 ± 1
18	**3e**	181 ± 1	>100	–	18.4 ± 1.2	Not tested
19	**3f**	163 ± 1	>100	–	16.9 ± 1.4	Not tested
20	**3g**	163 ± 1	0.22 ± 0.01	742	8.7 ± 0.1	7.1 ± 0.2
21	**3h**	117 ± 1	78 ± 1	2	6.4 ± 0.1	8.4 ± 0.1
22	**3i**	118 ± 1	>100	–	16.7 ± 1.2	Not tested
23	**4a**	155 ± 1	3.6 ± 0.2	43	15 ± 2	Not tested
24	**4b**	106 ± 1	5.1 ± 0.1	21	24.6 ± 1.3	Not tested
25	**4c**	137 ± 1	7.8 ± 0.1	18	18.4 ± 1.2	Not tested
26	**4d**	40 ± 1	>100	–	12 ± 2	Not tested
27	**4e**	189 ± 1	6.7 ± 0.9	28	11.2 ± 1.7	Not tested
28	**QR**	254 ± 1	0.56 ± 0.01	453	8.72 ± 0.1	5.1 ± 0.1
29	**OMV**	713 ± 1	(12.7 ± 0.3) × 10^3	5.6 × 10^4	(1.9 ± 0.1) × 10^3	(2.8 ± 0.3) × 10^4

MTT assay and crystal violet experiments performed in triplicates to give CC_{50} and EC_{50} values respectively, NA-inhibition and enzyme kinetics experiments performed in duplicates to give IC_{50} and Ki values respectively; CC_{50} (mean ± std dev) values represent the concentration of molecules that showed 50% cytotoxicity; EC_{50} (mean ± std dev) values represent the concentration that resulted in 50% cell survival after infection in presence of inhibitor; SI = Selectivity Index was generated by the ratio of CC_{50} and EC_{50}; IC_{50} (mean ± std dev) values of molecules represent the concentration that caused 50% enzyme activity loss; Ki represents the enzyme inhibitor constant.

Burk plot of 1/V versus 1/[S] resulted in group of lines as observed in **QR**, signifying their mechanism of enzyme inhibition to be non-competitive. Fig. 7 displays the plot for the representative potent molecules.

Table 3
Reductions of %HA titer of pdmH1N1 virus by aurone (**1a-1e**), 3-indolinone (**2a-2h**), 4-quinolone (**3a-3i**), CAPi hybrids (**4a-4e**); and standard competitive and non-competitive inhibitors oseltamivir phosphate and quercetin, respectively.

Molecules	HA titer Reduction (%)[a]	Molecules	HA titer Reduction (%)[a]
1a	31 ± 2%	**3c**	17 ± 1%
1b	82 ± 5%	**3d**	20 ± 2%
1c	64 ± 3%	**3e**	19 ± 2%
1d	81 ± 4%	**3f**	30 ± 3%
1e	12 ± 2%	**3g**	82 ± 5%
2a	75 ± 4%	**3h**	20 ± 2%
2b	70 ± 3%	**3i**	54 ± 2%
2c	70 ± 3%	**4a**	52 ± 2%
2d	60 ± 2%	**4b**	58 ± 3%
2e	63 ± 4%	**4c**	41 ± 2%
2f	89 ± 4%	**4d**	54 ± 2%
2g	65 ± 3%	**4e**	42 ± 3%
2h	72 ± 4%	**OMVP**	85 ± 4%
3a	84 ± 4%	**QR**	79 ± 4%
3b	50 ± 2%		

[a] Reduction of %HA titer of pdmH1N1 virus (mean ± std dev of three experiments) in presence of 100 μM of inhibitors, measured by hemagglutination inhibition assay.

2.4. Induced fit docking (IFD)

IFD is an accurate and robust docking technique that takes into account the ligand and protein flexibility. Validation of IFD process was done by superimposing the docked oseltamivir structure over the oseltamivir obtained from crystal structure of NA enzyme (PDB 3TI6). RMSD value for all the heavy atoms was obtained as 0.17 Å. Furthermore, the receptor binding of oseltamivir was found similar to that in the crystal structure. The interactions formed by both crystal structure and docked oseltamivir are: amide functional group of oseltamivir forming H-bond with R152; amino group forming salt bridges with E119, D151 and E277 and H-bond with E119 and E227; carboxylate moiety forming H-bonds with R118, R292 and R371 as shown in Fig. 1**b** (*vide supra*). IFD was executed on five most potent molecules to have an insight towards the accurate binding of these molecules when the enzyme is in its optimal conformation. IFD scores were found to be consistent with experimental CV assay results as shown in Table 4**.**

2.5. Structure-activity relationship (SAR)

All the deigned scaffolds fitted well in the 430-cavity which was believed to be the alternate binding region within the catalytic active site. However, the scaffolds exhibited varied degree of anti-influenza activity. The prototype scaffold selected i.e., chalcone, having uncyclized α, β-unsaturated carbonyl system, showed weaker anti-influenza activity as evident from literature. Comprehensive examination of the anti-influenza evaluation of our designed scaffolds suggested that cyclization of chalcone not only reduced cytotoxicity but also caused the improvement in activity. It was observed that 5-exo cyclocondensation of 2-amino chalcone to yield 3-indolinone enhanced the activity than 6-endo cyclocondensation to yield 4-quinolone. 3-indolinones were found to be even more active than the oxidative cyclized product of 2-hydroxy chalcone *viz.* aurone. Thus, it can be said that the isosteric replacement of nitrogen in 3-indolinone to oxygen in aurone reduced the activity. Incorporation/presence of phenyl rings provides hydrophobic sites for interaction between inhibitor molecule and the enzyme. The higher activity of 3-indolinones, 4-quinolones and aurones may be attributed to the presence of another phenyl ring that imparted more hydrophobicity to the molecules indicating towards their prominent interactions with the hydrophobic 430-cavity in docking studies. At the same time, when cinnamic acid (scaffold similar to chalcone having α, β-unsaturated carbonyl system) was linked to piperazine moiety, it improved the activity than cinnamic acid itself. This may be attributed to decrease in the

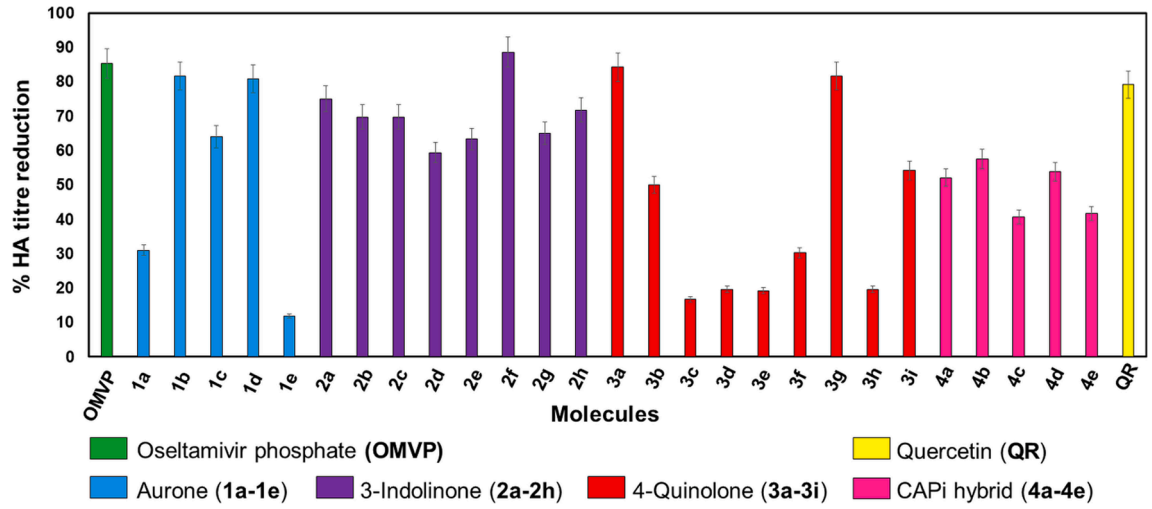

Fig.4. Histogram of % HA titer reduction of virus treated with candidate molecules showing the effect of oseltamivir phosphate (**OMVP**, green colour), quercetin (**QR**, yellow colour) and evaluated molecules on pdmH1N1 virus yield. (For interpretation of the references to colour in this figure legend, the reader is referred to the web version of this article.)

acidity of the molecule. The scaffolds were designed by substitution of various electron-withdrawing and electron-donating groups. Among tested molecules, substituting the benzyl ring with chloro group enhanced activity, out of which *meta* and *para* substituted chloro group containing 3-indolinones, **2f** and **2g** respectively, showed potency better than oseltamivir. While for 4-quinolones, electron-donating methoxy group at *ortho* position (**3a**) showed better activity than oseltamivir.

Hence, it can be said that for 5-exo cyclocondensation of chalcones, chloro group substitution at benzyl ring enhanced the activity while for 6-endo cyclocondensation, methoxy group substitution at phenyl ring showed better activity than the standard drug. Overall SAR studies pointed towards a better understanding of effect of presence of phenyl ring at 1–2 carbon lengths, 5-exo cyclocondensation, chloro substitution along with decreased acidity of the designed molecules towards their anti-influenza activity against influenza A/H1N1pdm09 virus.

Interesting to note here is that the active site of NA comprises of 430-cavity where our designed molecules bound. This binding region is distinctly different from oseltamivir and sialic acid binding site. Therefore, the molecules displayed non-competitive nature of inhibition. Since, this binding region of the molecules is adjacent to catalytic site and is present within the same active site, these molecules could correspondingly be called “mutually non-competitive” agents.

3. Conclusion

In current backdrop of COVID pandemic, our research is focused on another pandemic virus *viz.* swine flu – pandemic H1N1, which created havoc in 2009. Although, the current floating strains are not virulent and vaccine is available for its defense but the lesson learnt from COVID crisis is not to underestimate the strength of the virus. The impulsiveness of a potential influenza A pandemic outbreak and rapid unpredictable emergence of influenza A virus resistance to current anti-influenza drugs are urging the researchers and scientists to come up with newer strategies to overcome resistance and develop better options in terms of treatment than what current drugs can offer us. Based on the results obtained in the present study, we can say that subset of the drug molecules showed substantial antiviral activity against influenza A/H1N1pdm09 virus. Computational studies identified the molecules as binders of 430-cavity, an alternate binding region within the active site, similar to quercetin which was the standard for non-competitive inhibition, but distinct from OMV in SA binding site which was the standard for competitive inhibition. The non-cytotoxic molecules efficiently reduced the viral titer and remarkably restricted viral replication more actively than inhibiting the NA enzyme alone. Among the tested molecules, **2f**, **2g** and **3a** were found to be most potent anti-influenza agents having low-nanomolar EC_{50} values 4.02 nM, 6.72 nM and 4.96 nM, respectively, that were better compared to reference competitive and non-competitive inhibitors: oseltamivir (EC_{50} = 12.7 nM) and quercetin (EC_{50} = 0.56 μM). **2f, 2g** and **3a** also exhibited good NA inhibitory activity in sub-micromolar range (IC_{50} = 0.52 μM, 3.46 μM, 1.31 μM respectively). In addition, enzyme kinetics studies suggested that the mechanism of inhibition of our designed molecules is non-competitive that was highlighted by *in-silico* studies as well wherein the molecules bound to the alternate binding site. Owing to the fact that current commercial drugs work like charm in wild-type influenza, the potent molecules of present study can therefore be certainly used as an adjunct therapy in combination with oseltamivir or zanamivir for improved antiviral efficiency. This further strengthens our idea of developing potential anti-influenza agents in future which can be used as an alternative in wake of oseltamivir resistance owing to their non-competitive inhibition mechanism.

Thus, it can be concluded that the current work has generated few potential anti-influenza molecules especially for influenza A/H1N1pdm09 strain. The approach used here is completely different than the currently available marketed drugs. The potent molecules can be subsequently developed to be used either alone or in combination with current NA inhibitors for better management and eradication of influenza virus.

4. Experimental section

4.1. Materials

The chemicals, reagents and catalyst Amberlyst-15 employed for synthesis were purchased from SD Fine chem Ltd. and Sigma Aldrich Chemicals Pvt Ltd. All the solvents used for synthesis were of LR grade. Oseltamivir phosphate (OMVP) was obtained as a gift sample from Cipla Ltd, India. Oseltamivir carboxylate (OMVC) and quercetin (QR) was purchased from Clearsynth Labs, Ltd and Sigma Aldrich Chemicals Pvt Ltd, respectively. The strain of A(H1N1)pdm09 virus Kolkata isolate [A/human/India/Kol-7251/2018(H1N1); accession number: MN508979] was obtained from ICMR-National Institute of Cholera and Enteric Diseases (ICMR-NICED), Kolkata, India. Madin-Darby Canine Kidney (MDCK) cells were obtained from National Institute of Virology (NIV), Pune, India.

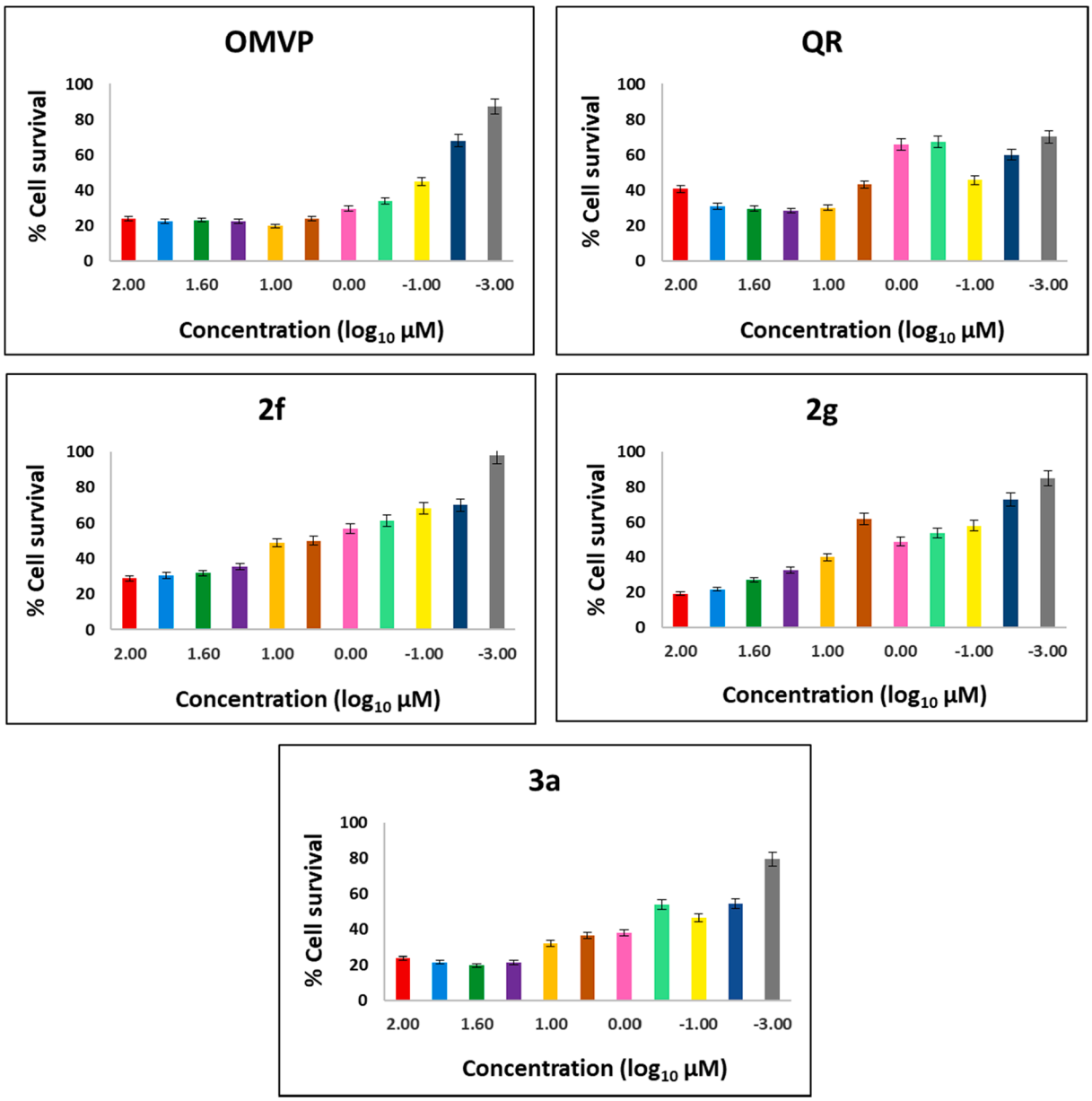

Fig.5. Effects of oseltamivir phosphate (**OMVP**), quercetin (**QR**) and representative potent molecules **2f, 2g** and **3a** on % cell survival infected with H1N1 virus.

4.2. Methods

4.2.1. Modelling and system preparation for modelling

The X-ray crystal structure of OMV-complexed pandemic H1N1-NA enzyme was imported from RCSB protein data bank (PDB ID: 3TI6), with a resolution of 1.69 Å [32]. Since NA is a homotetramer, monomer unit of the enzyme (3TI6) was considered for docking calculations in computational studies. Protein Preparation Wizard module of Maestro 11.5, Schrödinger LLC, New York, USA [49] was employed to optimize the geometry of the enzyme. The crystallographic waters were removed, hydrogen atoms were added to the enzyme structure consistent with a pH of 6.5, which is the optimum pH for NA enzymatic activity [50]. N- and C-termini were capped. Ca^{2+} is reported to be crucial for enzyme activity and stability, therefore, two Ca^{2+} ions were retained: one whose binding site is close to the active site which helps in holding the active site in appropriate conformation for substrate binding; while the other whose binding site was found in 1918 N1 and 2009 swine-origin N1 structures [50,51]. The terminal rotamer states were set automatically for Asn, Gln and His, as well as tautomeric and protonation states of His to optimize the hydrogen-bonding network in the complex using ProtAssign program in Maestro. Minimization was implemented using OPLS3e forcefield.

SiteMap [36,52] tool was applied to explore the potential binding sites and characterize them. Different molecules were designed with introducing substituents with varied functional groups attributing electronic, steric and volume effect to the scaffolds. All the designed molecules were built using the 2D sketcher available with Maestro 11.5 (Schrödinger LLC NY 2016) and their geometries were optimised using LigPrep v3 module [53] with OPLS3e forcefield and docked in the putative binding sites using Glide XP [35,54]. Best docking scores were for the molecules showing binding in the 430-cavity of influenza A/H1N1pdm09-NA enzyme than other putative binding pockets. Additionally, induced fit docking (IFD) [55] of the best molecules was executed in this binding pocket since the receptor may not be in an optimal conformation to bind the inhibitor molecules. The validation of docking protocol was done by replicating the binding pose and interactions of co-crystallized ligand i.e., oseltamivir in the X-ray crystal structure.

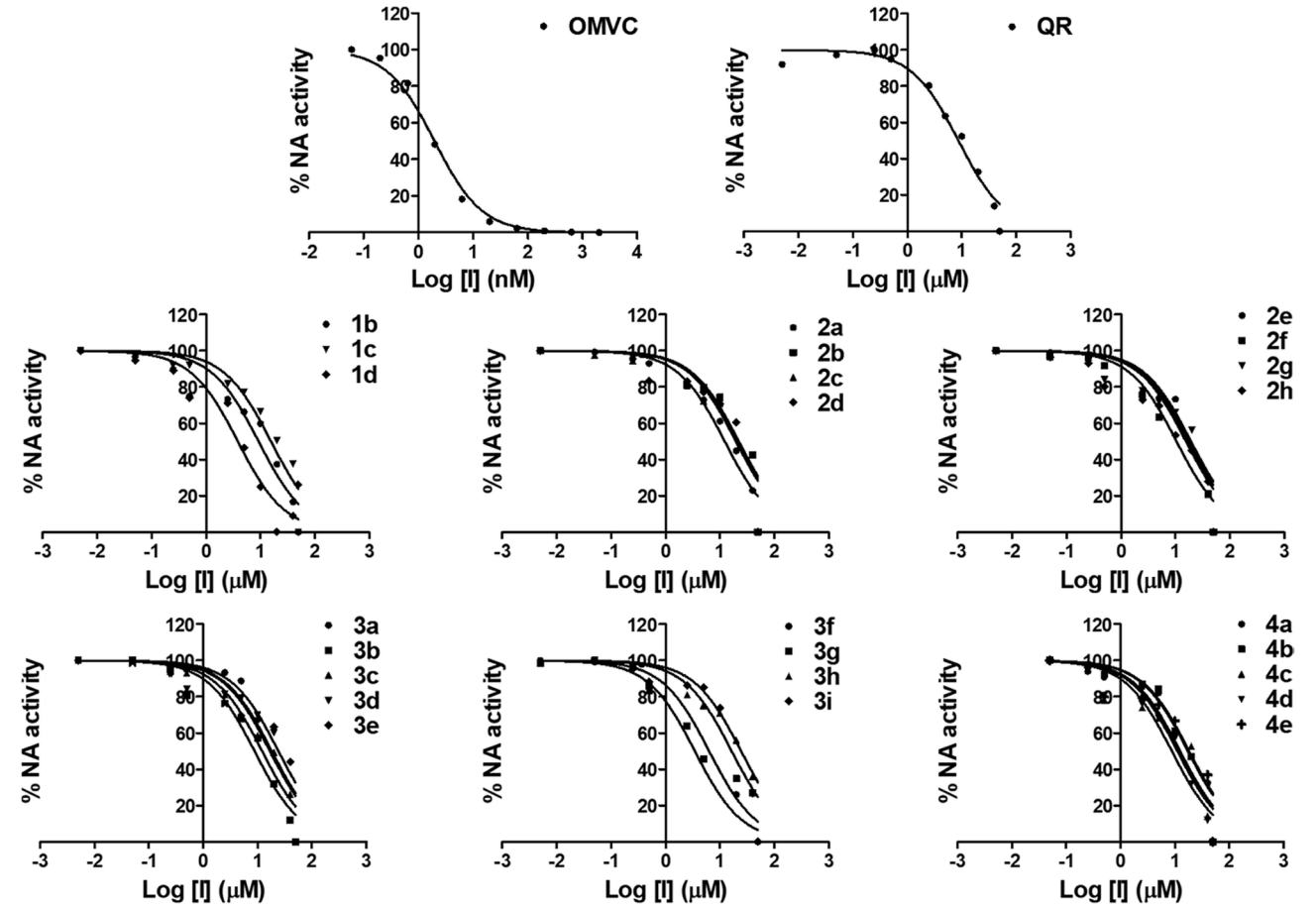

Fig.6. Effects of oseltamivir carboxylate (**OMVC**), quercetin (**QR**) and evaluated molecules on H1N1-NA for the hydrolysis of substrate.

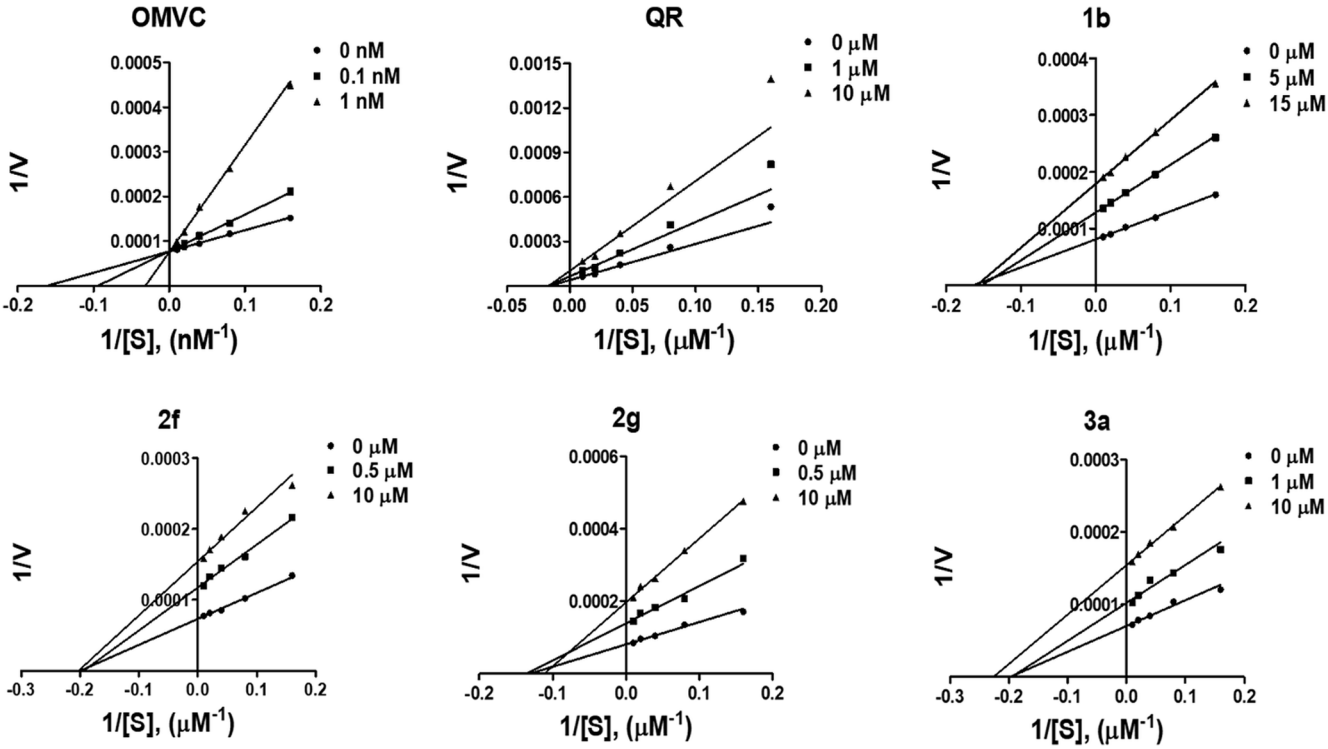

Fig.7. Lineweaver–Burk plots for the inhibition of oseltamivir carboxylate (**OMVC**), quercetin (**QR**) and representative evaluated molecules on H1N1-NA for the hydrolysis of substrate in the presence of increasing concentrations of tested molecules (two conc. bracketing IC_{50}) for lines from bottom to top.

Table 4
IFD scores, EC_{50} and IC_{50} values of potent inhibitor molecules.

Molecules	EC_{50} (μM)	IC_{50} (μM)	IFD scores
2f	$(4.0 \pm 0.1) \times 10^3$	0.52 ± 0.01	−861.6
2g	$(6.7 \pm 0.1) \times 10^3$	3.5 ± 0.1	−858.9
3a	$(4.9 \pm 0.1) \times 10^3$	1.3 ± 0.2	−860.5
QR	0.56 ± 0.01	8.7 ± 0.1	−857.7
OMV	$(12.7 \pm 0.3) \times 10^3$	$(1.9 \pm 0.1) \times 10^3$	−858.0

The physicochemical properties, *viz.* absorption, distribution, metabolism and elimination (ADME), of the designed molecules were predicted *in-silico* by QikProp 3.3 (Schrödinger LLC, New York, USA) [56]. The out file of LigPrep, employed to optimize the designed molecules, was employed as the input for QikProp to predict the molecular descriptors as well as properties of the molecules that are physically significant and pharmaceutically relevant. Comparison between properties of the designed molecules with those of 95% of overall known drugs was done using the range values of each molecular descriptor provided by QikProp.

4.2.2. Chemistry

The starting materials and solvents utilized for synthesis were assessed for their purity by determining their physical constants (*viz.* melting and boiling point) and by thin-layer chromatography (TLC) on Merck silica gel F_{254} plates. We report here the synthesis of four scaffolds namely aurones, 3-indolinones, 4-quinolones and CAPi hybrids (Scheme 1 and Scheme 2). Synthesis was carried out in Carousel 6-reaction station parallel synthesizer by Radleys. TLC was employed to monitor the synthetic reaction progress. Physical constants (melting point) of the reaction products were determined by Analab melting point apparatus μThermoCal10. Infrared spectroscopy (IR), ^{1}H NMR and ^{13}C NMR were employed for structural characterization of the synthesized molecules. Mass spectra (MS) and HPLC purity of the synthesized molecules were measured as well. IR experiments were recorded on an inhouse Bruker Alpha-T spectrometer with 44 scans, and data were processed by OPUS software. NMR experiments were recorded on 800 MHz Bruker Avance spectrometer and 600 MHz Varian spectrometer using DMSO-d_6 and $CDCl_3$ solvent, and the data were processed using Bruker Topspin 2.1 and Varian software. 64 scans were recorded for 1D proton NMR (in 600 MHz NMR spectrometer), while for carbon NMR, 2064 scans (in 150 MHz NMR spectrometer) and 500 scans (in 200 MHz NMR spectrometer) were recorded. LC-MS/MS were recorded on Water make Mass Spectrometry LCMS: water alliance quadrupole mass. HPLC was performed on Agilent 1200 series HPLC system.

*4.2.2.1. General procedure for synthesis of aurones (**1a**–**1e**).* 2-Hydroxychalcones were primarily synthesized followed by their oxidative cyclization to obtain aurones (Scheme 1). 2-Hydroxychalcones and mercuric acetate [$Hg(OAC)_2$] were dissolved in pyridine (15–20 mL) in equimolar (0.002 mol) quantities at 27 °C. The reaction mixture was kept on stirring at 110 °C for 1–2 h. Completion of reaction was monitored by TLC (Hexane:Ethyl acetate; 3:2). The cooled reaction mixture was poured into ice-cold water and acidified with dil. HCl (10% aqueous solution). The precipitated solid was extracted with dichloromethane or ethyl acetate, the extracts were dried over sodium sulphate bed and the solvent was evaporated to give a solid which was recrystallized from absolute ethanol.

(Z)-2-(3′-Methoxy-benzylidene)-benzofuran-3-one (1a). Yellow solid, yield (64%), m.p. 117–120 °C. ^{1}H NMR (DMSO-d_6, 600 MHz, 25 °C, TMS) δ ppm 7.81–7.78 (d, t, 2H, H-4, H-5), 7.59–7.55 (d, d, s, 3H, H-6′, H-7, H-2′), 7.43–7.40 (t, 1H, H-5′), 7.33–7.30 (t, 1H, H-6), 7.04–7.03 (d, 1H, H-4′), 6.90 (s, 1H, H-10), 3.81 (s, 3H, OCH_3); ^{13}C NMR (DMSO-d_6, 200 MHz, 25 °C, TMS) δ ppm 184.15 (C═O, C-3), 165.96 (C, C-3′), 159.92 (C, C-8), 146.86 (C, C-2), 138.21 (C, C-1′), 133.58 (CH, C-6), 130.55 (CH, C-4), 124.80 (CH, C-5′), 121.28 (C, C-9), 117.12 (CH, C-5), 116.29 (CH, C-4′), 113.76 (CH, C-10), 112.63 (CH, C-2′), 55.66 (OCH_3). MS: calcd for $C_{16}H_{12}O_3$ m/z = 252, found 253.1. HPLC peak purity: 99.6%.

(Z)-2-(4′-Methoxy-benzylidene)-benzofuran-3-one (1b). Yellow solid, yield (52%), m.p. 137–139 °C. ^{1}H NMR (DMSO-d_6, 600 MHz, 25 °C, TMS) δ ppm 7.96–7.94 (d, 2H, H-2′, H-6′), 7.78–7.75 (d, t, 2H, H-4, H-5), 7.53–7.52 (d, 1H, H-7), 7.31–7.28 (t, 1H, H-6), 7.08–7.06 (d, 2H, H-3′, H-5′), 6.91 (s, 1H, H-10), 3.82 (s, 3H, OCH_3); ^{13}C NMR (DMSO-d_6, 200 MHz, 25 °C, TMS) δ ppm 183.74 (C═O, C-3), 165.61 (C, C-4′), 161.34 (C, C-8), 145.63 (C, C-2), 137.79 (CH, C-6), 133.89 (CH, C-4), 124.90 (CH, C-2′, C-6′), 124.64 (C, C-1′), 124.28 (CH, C-9), 121.62 (CH, C-5), 115.195 (CH, C-7), 113.65 (CH, C-10), 113.23 (CH, C-3′, C-5′), 55.88 (OCH_3). MS: calcd for $C_{16}H_{12}O_3$ m/z = 252, found 253.1. HPLC peak purity: 97.3%.

(Z)-2-(3′-Chloro-benzylidene)-benzofuran-3-one (1c). Yellow solid, yield (53%), m.p. 165–168 °C. ^{1}H NMR (DMSO-d_6, 600 MHz, 25 °C, TMS) δ ppm 8.02 (s, 1H, H-2′), 7.95–7.94 (d, 1H, H-6′), 7.82–7.78 (d, t, 2H, H-4, H-5), 7.58–7.56 (d, 1H, H-7), 7.54–7.50 (d, t, 2H, H-4′, H-5′), 7.34–7.31 (t, 1H, H-6), 6.93 (s, 1H, H-10). MS: calcd for $C_{15}H_9O_2Cl$ m/z = 256.5, found 257.0. HPLC peak purity: 98.7%.

(Z)-2-(4′-Chloro-benzylidene)-benzofuran-3-one (1d). Yellow solid, yield (62%), m.p. 154–160 °C. ^{1}H NMR (DMSO-d_6, 600 MHz, 25 °C, TMS) δ ppm 8.00–7.99 (d, 2H, H-2′, H-6′), 7.81–7.79 (d, t, 2H, H-4, H-5), 7.57–7.53 (d, d, 3H, H-3′, H-5′, H-7), 7.33–7.30 (t, 1H, H-6), 6.94 (s, 1H, H-10); ^{13}C NMR (DMSO-d_6, 150 MHz, 25 °C, TMS) δ ppm 183.59 (C═O, C-3), 165.44 (C, C-8), 146.47 (C, C-2), 137.87 (CH, C-6), 134.65 (C, C-4′), 132.97 (C, C-1′), 130.86 (C, C-4), 129.21 (CH, C-3′, C-5′), 124.44 (CH, C-2′, C-6′), 124.19 (C, C-9), 120.74 (CH, C-5), 113.31 (CH, C-7), 111.04 (CH, C-10). MS: calcd for $C_{15}H_9O_2Cl$ m/z = 256.5, found 257.1. HPLC peak purity: 97.4%.

(Z)-2-(4′-Nitro-benzylidene)-benzofuran-3-one (1e). Yellow solid, yield (48%), m.p. 211–215 °C. ^{1}H NMR (DMSO-d_6, 600 MHz, 25 °C, TMS) δ ppm 8.40–8.38 (d, 2H, H-3′, H-5′), 8.26–8.25 (d, 2H, H-2′, H-6′), 7.82–7.79 (d, t, 2H, H-4, H-5), 7.58–7.56 (d, 1H, H-7), 7.36–7.33 (t, 1H, H-6), 7.11 (s, 1H, H-10). MS: calcd for $C_{15}H_9NO_4$ m/z = 267, found 268.0.

*4.2.2.2. General procedure for synthesis of 3-indolinones (**2a- 2h**).* The scheme is based on 5-exo cyclic condensation of 2-amino chalcone in presence of Amberlyst-15 as a catalyst [57] as shown in Scheme 1. 0.075 mol of 2-amino chalcone derivatives were dissolved in 3–5 mL of acetic acid. To this solution 10% w/w Amberlyst-15 was added. The mixture was stirred at 80 °C for 2–5 h until starting material was not detected by TLC (Hexane:Ethyl acetate; 3:2). The product was filtered and recrystallized from absolute ethanol. The catalyst was obtained back by washing with methanol, which could be reused.

(Z)-2-(2′-Methoxy-benzylidene)-1,2-dihydro-indol-3-one (2a). Pale yellow solid, yield (52%), m.p. 173–175 °C. ^{1}H NMR (DMSO-d_6, 600 MHz, 25 °C, TMS) δ ppm 11.24 (s, 1H, NH), 7.93 (d, 1H, H-4), 7.67 (d, 1H, H-6′), 7.60 (d, 1H, H-7), 7.52 (t, 1H, H-6), 7.35 (t, 1H, H-4′), 7.00–6.90 (m, 4H, H-3′, H-5, H-5′, H-10), 3.69 (s, 3H, OCH_3); ^{13}C NMR (DMSO-d_6, 200 MHz, 25 °C, TMS) δ ppm 186.30 (C═O, C-3), 157.49 (C, C-2′), 144.97 (C, C-2), 135.61 (CH, C-6), 135.21 (C, C-8), 133.53 (CH, C-4′), 128.25 (CH, C-6′), 124.01 (CH, C-4), 123.01 (CH, C-5′), 122.57 (C, C-1′), 121.41 (C, C-9), 119.61 (CH, C-5), 112.81 (CH, C-7), 111.91 (CH, C-3′), 108.38 (C-10), 54.53 (OCH_3). MS: calcd for $C_{16}H_{13}NO_2$ m/z = 251, found 250.96. HPLC peak purity: 99.7%.

(Z)-2-(3′-Methoxy-benzylidene)-1,2-dihydro-indol-3-one (2b). Pale yellow solid, yield (64%), m.p. 117–120 °C. ^{1}H NMR (DMSO-d_6, 600 MHz, 25 °C, TMS) δ ppm 11.26 (s, 1H, NH), 7.94 (d, 1H, H-4), 7.62 (d, 1H, H-7), 7.53 (t, 1H, H-6′), 7.24–7.19 (m, 3H, H-2′, H-5′, 6′), 6.96 (t, 1H, H-5), 6.86 (d, 1H, H-4′), 6.65 (s, 1H, H-10), 3.65 (s, 3H, OCH_3); ^{13}C NMR (DMSO-d_6, 200 MHz, 25 °C, TMS) δ ppm 188.23 (C═O, C-3), 159.72 (C, C-3′), 144.37 (C, C-2), 137.06 (C, C-8), 136.67 (C, C-1′), 135.61 (CH, C-6), 126.61 (CH, C-5′), 125.01 (CH, C-6′), 124.01 (CH, C-

4), 121.24 (C, C-9), 119.61 (CH, C-5), 114.79 (CH, C-4′), 114.65 (CH, C-2′), 112.81 (CH, C-7), 110.41 (CH, C-10), 55.25 (OCH_3). MS: calcd for $C_{16}H_{13}NO_2$ m/z = 251, found 253.98. HPLC peak purity: 99.5%.

(Z)-2-(4′-Methoxy-benzylidene)-1,2-dihydro-indol-3-one (2c). Pale yellow solid, yield (52%), m.p. 137–140 °C. ^{1}H NMR (DMSO-d_6, 600 MHz, 25 °C, TMS) δ ppm 11.25 (s, 1H, NH), 7.94 (d, 1H, H-4), 7.62 (d, 1H, H-7), 7.55–7.49 (t, d, 3H, H-6, H-2′, H-6′), 6.97–6.95 (d, 3H, H-5, H-3′, H-5′), 6.64 (s, 1H, H-10), 3.70 (s, 3H, OCH_3); ^{13}C NMR (DMSO-d_6, 150 MHz, 25 °C, TMS) δ ppm 188.23 (C═O, C-3), 159.85 (C, C-4′), 145.34 (C, C-2), 137.06 (C, C-8), 135.61 (CH, C-6), 130.22 (CH, C-2′, C-6′), 129.72 (C, C-1′), 124.01 (CH, C-4), 121.24 (C, C-9), 119.61 (CH, C-5), 113.98 (CH, C-3′, C-5′), 112.81 (CH, C-7), 110.56 (CH, C-10), 55.35 (OCH_3). MS: calcd for $C_{16}H_{13}NO_2$ m/z = 251, found 254.30. HPLC peak purity: 99.2%.

(Z)-2-(3′, 4′, 5′-Trimethoxy-benzylidene)-1,2-dihydro-indol-3-one (2d). Pale yellow solid (56%), m.p. 138–141 °C. ^{1}H NMR (DMSO-d_6, 600 MHz, 25 °C, TMS) δ ppm 11.25 (s, 1H, NH), 7.93 (d, 1H, H-4), 7.62 (d, 1H, H-7), 7.52 (t, 1H, H-6), 6.95 (t, 1H, H-5), 6.84 (s, 2H, H-2′, H-6′), 6.64 (s, 1H, H-10), 3.73–3.64 (d, 9H, OCH_3); ^{13}C NMR (DMSO-d_6, 150 MHz, 25 °C, TMS) δ ppm 188.23 (C═O, C-3), 154.24 (C, C-3′, C-5′), 144.29 (C, C-2), 143.34 (C, C-4′), 137.06 (C, C-8), 135.61 (CH, C-6), 131.95 (C, C-1′), 124.01 (CH, C-4), 121.24 (C, C-9), 119.61 (CH, C-5), 112.81 (CH, C-7), 110.06 (CH, C-10), 107.52 (CH, C-2′, C-6′), 60.68–56.20 (OCH_3). MS: calcd for $C_{18}H_{17}NO_4$ m/z = 311, found 311.92. HPLC peak purity: 99.4%.

(Z)-2-(2′-Chloro-benzylidene)-1,2-dihydro-indol-3-one (2e). Pale yellow solid, yield (58%), m.p. 136–138 °C. ^{1}H NMR (DMSO-d_6, 600 MHz, 25 °C, TMS) δ ppm 10.91 (s, 1H, NH), 8.21 (d, 1H, H-4), 7.49 (d, 2H, H-3′, H-6′), 7.36–7.30 (m, 2H, H-6, H-4′), 7.24 (t, 1H, H-5), 7.20–7.16 (t, s, 2H, H-5′, H-10), 6.98 (d, 1H, H-7); ^{13}C NMR (DMSO-d_6, 150 MHz, 25 °C, TMS) δ ppm 181.92 (C═O, C-3), 148.98 (C, C-8), 138.01 (C, C-2′), 134.65 (C, C-1′), 133.47 (CH, C-6′), 129.59 (CH, C-4′), 129.47 (CH, C-6), 128.98 (CH, C-3′), 126.64 (C, C-2), 126.43 (CH, C-5′), 122.76 (CH, C-4), 121.10 (CH, C-5), 118.34 (C, C-9), 112.91 (CH, C-7), 104.28 (CH, C-10). MS: calcd for $C_{15}H_{10}NOCl$ m/z = 255.5, found 255.92. HPLC peak purity: 94.5%.

(Z)-2-(3′-Chloro-benzylidene)-1,2-dihydro-indol-3-one (2f). Pale yellow solid, yield (53%), m.p. 101–103 °C. ^{1}H NMR (DMSO-d_6, 600 MHz, 25 °C, TMS) δ ppm 10.65 (s, 1H, NH), 8.11 (d, 1H, H-4), 7.79 (d, 1H, H-6′), 7.60 (s, 1H, H-2′), 7.33–7.30 (t, 2H, H-4′, H-5′), 7.18 (t, 1H, H-5), 7.09 (t, 1H, H-6) 6.88–6.86 (d, 2H, H-7, H-10); ^{13}C NMR (DMSO-d_6, 200 MHz, 25 °C, TMS) δ ppm 180.04 (C═O, C-3), 148.95 (C, C-8), 135.11 (C, C-1′), 133.52 (C, C-3′), 133.21 (CH, C-2′), 131.13 (CH, C-6′), 130.65 (CH, C-4′), 129.47 (CH, C-6), 128.48 (CH, C-5′), 127.78 (C, C-2), 122.76 (CH, C-4), 121.10 (CH, C-5), 118.31 (C, C-9), 112.91 (CH, C-7), 107.98 (CH, C-10). MS: calcd for $C_{15}H_{10}NOCl$ m/z = 255.5, found 255.92. HPLC peak purity: 99.9%.

(Z)-2-(4′-Chloro-benzylidene)-1,2-dihydro-indol-3-one (2g). Pale yellow solid, yield (62%), m.p. 156–160 °C. ^{1}H NMR (DMSO-d_6, 600 MHz, 25 °C, TMS) δ ppm 10.67 (s, 1H, NH), 8.11 (d, 1H, H-4), 7.73 (d, 2H, H-2′, H-6′), 7.43 (d, 2H, H-3′, H-5′), 7.25 (t, 1H, H-6), 7.04 (t, 1H, H-5), 6.88–6.85 (d, 2H, H-7, H-10); ^{13}C NMR (DMSO-d_6, 200 MHz, 25 °C, TMS) δ ppm 180.02 (C═O, C-3), 148.95 (C, C-8), 135.41 (C, C-1′), 134.48 (CH, C-3′, C-5′), 132.16 (C, C-4′), 129.47 (CH, C-6), 129.22 (CH, C-2′, C-6′), 127.07 (CH, C-4), 122.76 (CH, C-5), 121.10 (C, C-9), 118.31 (CH, C-7), 112.91 (C, C-2), 107.68 (CH, C-10). MS: calcd for $C_{15}H_{10}NOCl$ m/z = 255.5, found 255.92. HPLC peak purity: 99.3%.

(Z)-2-(3′-Hydroxy-benzylidene)-1,2-dihydro-indol-3-one (2h). Pale yellow solid, yield (56%), m.p. 130–132 °C. ^{1}H NMR (DMSO-d_6, 600 MHz, 25 °C, TMS) δ ppm 11.26 (s, 1H, NH), 9.87 (s, 1H, OH), 7.94 (d, 1H, H-4), 7.62 (d, 1H, H-7), 7.53 (t, 1H, H-6), 7.14 (t, 1H, H-5′), 7.07 (d, 1H, H-6′), 6.96 (t, 1H, H-5), 6.65–6.63 (d, 3H, H-2′, H-4′, H-10); ^{13}C NMR (DMSO-d_6, 200 MHz, 25 °C, TMS) δ ppm 188.23 (C═O, C-3), 156.32 (C, C-3′), 144.37 (C, C-2), 137.06 (CH, C-8), 136.74 (C, C-1′), 135.61 (CH, C-6), 130.04 (CH, C-5′), 124.85 (CH, C-6′), 124.01 (CH, C-4), 121.24 (C, C-9), 119.69 (CH, C-2′), 119.61 (CH, C-5), 116.55 (CH, C-4′), 112.81 (CH, C-7), 110.41 (CH, C-10). MS: calcd for $C_{15}H_{11}NO_2$ m/z = 237, found 237.99.

*4.2.2.3. General procedure for synthesis of 4-quinolones (**3a–3i**).* 4-quinolones were obtained by 6-endo cyclocondensation of 2-amino chalcone derivatives using iodine and dimethylsulfoxide (DMSO) as shown in Scheme 1. 2-Amino chalcone derivatives were suspended in DMSO (10 mL) and a crystal of iodine was added to it. The reaction mixture was refluxed for 30 min and then diluted with water. The solid obtained was filtered off, washed with 20% sodium thiosulphate and recrystallized from absolute ethanol.

2-(2′-Methoxy-phenyl)-1H-quinolin-4-one (3a). White solid, yield (57%), m.p. 102–104 °C. ^{1}H NMR (DMSO-d_6, 600 MHz, 25 °C, TMS) δ ppm 11.50 (s, 1H, NH), 7.98 (d, 1H, H-6), 7.65 (d, 1H, H-9), 7.59–7.51 (t, t, 2H, H-7, H-8), 7.37 (d, 1H, H-6′), 7.28 (t, 1H, H-4′), 7.00 (d, 1H, H-3′), 6.94–6.88 (t, 1H, H-5′), 6.02 (s, 1H, H-3), 3.74 (s, 3H, OCH_3); ^{13}C NMR (DMSO-d_6, 200 MHz, 25 °C, TMS) δ ppm 182.44 (C═O, C-4), 155.01 (C, C-2′), 141.08 (C, C-10), 140.71 (C, C-2), 137.01 (CH, C-4′), 133.43 (CH, C-8), 130.32 (CH, C-6′), 125.01 (CH, C-6), 124.21 (C, C-1′), 123.83 (C, C-5), 123.31 (CH, C-7), 122.88 (CH, C-5′), 119.07 (CH, C-9), 110.53 (CH, C-3′), 106.19 (CH, C-3), 55.20 (OCH_3). MS: calcd for $C_{16}H_{13}NO_2$ m/z = 251, found 251.99. HPLC peak purity: 99.9%.

2-(3′-Methoxy-phenyl)-1H-quinolin-4-one (3b). White solid, yield (64%), m.p. 130–134 °C. ^{1}H NMR (DMSO-d_6, 600 MHz, 25 °C, TMS) δ ppm 11.65 (s, 1H, NH), 8.09 (d, 1H, H-6), 7.76 (d, 1H, H-9), 7.71–7.63 (t, t, 2H, H-7, H-8), 7.45 (t, 1H, H-5′), 7.36 (d, 1H, H-6′), 7.27 (s, 1H, H-2′), 7.09 (d, 1H, H-4′), 6.31 (s, 1H, H-3), 3.75 (s, 3H, OCH_3); ^{13}C NMR (DMSO-d_6, 150 MHz, 25 °C, TMS) δ ppm 182.44 (C═O, C-4), 161.82 (C, C-3′), 156.61 (C, C-2), 141.64 (C, C-10), 138.82 (C, C-1′), 133.43 (CH, C-8), 125.01 (CH, C-6), 123.31 (CH, C-7), 122.56 (CH, C-4′), 122.41 (C, C-5), 119.61 (CH, C-6′), 118.41 (CH, C-2′), 115.36 (CH, C-9), 108.21 (CH, C-5′), 105.71 (CH, C-3), 55.50 (OCH_3). MS: calcd for $C_{16}H_{13}NO_2$ m/z = 251, found 251.97. HPLC peak purity: 97.6%.

2-(4′-Methoxy-phenyl)-1H-quinolin-4-one (3c). White solid, yield (64%), m.p. 156–159 °C. ^{1}H NMR (DMSO-d_6, 600 MHz, 25 °C, TMS) δ ppm 11.66 (s, 1H, NH), 8.09 (d, 1H, H-6), 7.84–7.80 (d, 2H, H-3′, H-5′), 7.76 (d, 1H, H-9), 7.71–7.63 (t, t, 2H, H-7, H-8), 7.13–7.12 (d, 2H, H-2′, H-6′), 6.32 (s, 1H, H-3), 3.75 (s, 3H, OCH_3); ^{13}C NMR (DMSO-d_6, 150 MHz, 25 °C, TMS) δ ppm 182.44 (C═O, C-4), 158.80 (C, C-4′), 151.79 (C, C-2), 141.66 (C, C-10), 133.43 (CH, C-8), 128.79 (CH, C-2′, C-6′), 128.29 (C, C-1′), 125.01 (CH, C-6), 123.31 (CH, C-7), 122.41 (C, C-5), 115.36 (CH, C-9), 114.33 (CH, C-3′, C-5′), 105.65 (CH, C-3), 55.35 (OCH_3). MS: calcd for $C_{16}H_{13}NO_2$ m/z = 251, found 251.97. HPLC peak purity: 96.7%.

2-(3′, 4′, 5′-Trimethoxy-phenyl)-1H-quinolin-4-one (3d). White solid, yield (75%), m.p. 162–164 °C. ^{1}H NMR (DMSO-d_6, 600 MHz, 25 °C, TMS) δ ppm 11.65 (s, 1H, NH), 8.09 (d, 1H, H-6), 7.77 (d, 1H, H-9), 7.71–7.63 (t, t, 2H, H-7, H-8), 6.92 (s, 2H, H-2′, H-6′), 6.31 (s, 1H, H-3), 3.84–3.75 (d, 9H, OCH_3); ^{13}C NMR (DMSO-d_6, 150 MHz, 25 °C, TMS) δ ppm 182.44 (C═O, C-4), 153.72 (C, C-3′), 152.86 (C, C-2, 5′), 141.68 (C, C-10, C-4′), 141.64 (CH, C, C-8, C-1′), 133.43 (CH, C-6), 125.01 (CH, C-7), 123.31 (C, C-5), 122.41 (CH, C-9), 115.36 (CH, C-3), 104.99 (CH, C-2′), 104.08 (CH, C-6′), 60.68–56.26 (OCH_3). MS: calcd for $C_{18}H_{17}NO_4$ m/z = 311, found 311.91. HPLC peak purity: 99.8%.

2-(2′-Chloro-phenyl)-1H-quinolin-4-one (3e). Off-white solid, yield (56%), m.p. 116–119 °C. ^{1}H NMR (DMSO-d_6, 600 MHz, 25 °C, TMS) δ ppm 11.62 (s, 1H, NH), 8.09 (d, 1H, H-6), 7.76 (d, 1H, H-9), 7.70 (t, 1H, H-8), 7.64 (t, 1H, H-7), 7.59 (d, 1H, H-3′), 7.49 (t, 1H, H-4′), 7.42 (d, 1H, H-6′), 7.24 (t, 1H, H-5′), 6.14 (s, 1H, H-3); ^{13}C NMR (DMSO-d_6, 150 MHz, 25 °C, TMS) δ ppm 182.44 (C═O, C-4), 141.08 (C, C-10), 140.53 (C, C-2), 136.39 (C, C-1′), 133.43 (C, C-2′), 133.29 (CH, C-8), 130.79 (CH, CC-4′), 129.90 (CH, C-3′), 129.40 (CH, C-6′), 126.00 (CH, C-5′), 125.01 (CH, C-6), 123.83 (C, C-5), 123.31 (CH, C-7), 119.07 (CH, C-9), 113.95 (CH, C-3). MS: calcd for $C_{15}H_{10}NOCl$ m/z = 255.5, found 258.90. HPLC peak purity: 96.7%.

2-(3′-Chloro-phenyl)-1H-quinolin-4-one (3f). Off-white solid, yield (53%), m.p. 109–110 °C. ^{1}H NMR (DMSO-d_6, 600 MHz, 25 °C, TMS) δ ppm 11.55 (s, 1H, NH), 7.99 (d, 1H, H-6), 7.66 (d, 1H, H-9), 7.61–7.53 (t, t, 2H, H-7, H-8), 7.46 (d, 1H, H-6′), 7.3–7.2 (m, 3H, H-2′, H-4′, H-5′), 6.21 (s, 1H, H-3); ^{13}C NMR (DMSO-d_6, 150 MHz, 25 °C, TMS) δ ppm 182.44 (C═O, C-4), 156.61 (C, C-2), 141.64 (C, C-10), 138.36 (CH, C-1′), 134.03 (C, C-3′), 133.43 (CH, C-8), 130.39 (CH, C-4′), 129.51 (CH, C-5′), 128.68 (CH, C-2′), 125.20 (CH, C-6′), 125.01 (CH, C-6), 123.31 (CH, C-7), 122.41 (C, C-5), 115.36 (CH, C-9), 105.71 (CH, C-3). MS: calcd for $C_{15}H_{10}NOCl$ m/z = 255.5, found 255.28. HPLC peak purity: 85.5%.

2-(4′-Chloro-phenyl)-1H-quinolin-4-one (3 g). Off-white solid, yield (59%), m.p. 170–179 °C. ^{1}H NMR (DMSO-d_6, 600 MHz, 25 °C, TMS) δ ppm 11.66 (s, 1H, NH), 8.09 (d, 1H, H-6), 7.84–7.83 (d, 2H, H-3′, H-5′), 7.76 (d, 1H, H-9), 7.71–7.63 (t, t, 2H, H-7, H-8), 6.92–6.91 (d, 2H, H-2′, H-6′), 6.32 (s, 1H, H-3); ^{13}C NMR (DMSO-d_6, 200 MHz, 25 °C, TMS) δ ppm 182.44 (C═O, C-4), 151.79 (C, C-2), 141.66 (C, C-10), 135.80 (C, C-1′), 134.23 (C, C-4′), 133.43 (CH, C-8), 129.41 (CH, C-3′, C-5′), 129.22 (CH, C-2′, C-6′), 125.01 (CH, C-6), 123.31 (CH, C-7), 122.41 (C, C-5), 115.36 (CH, C-9), 105.65 (CH, C-3). MS: calcd for $C_{15}H_{10}NOCl$ m/z = 255.5, found 255.91. HPLC peak purity: 99.3%.

2-(3′-Nitro-phenyl)-1H-quinolin-4-one (3 h). Pale yellow solid, yield (49%), m.p. 195–196 °C. ^{1}H NMR (DMSO-d_6, 600 MHz, 25 °C, TMS) 11.53 (s, 1H, NH), 8.02–7.9 (m, 3H, H-6, H-4′, H-6′), 7.73 (s, 1H, H-2′), 7.65 (d, 1H, H-9), 7.60–7.52 (t, t, 2H, H-7, H-8), 7.45 (t, 1H, H-5′), 6.21 (s, 1H, H-3); ^{13}C NMR (DMSO-d_6, 200 MHz, 25 °C, TMS) δ ppm 182.44 (C═O, C-4), 156.61 (C, C-2), 147.93 (C, C-3′), 141.64 (C, C-10), 138.46 (C, C-1′), 133.82 (CH, C-5′), 133.43 (CH, C-8), 128.82 (CH, C-6′), 125.21 (CH, C-4′), 125.01 (CH, C-6), 123.47 (CH, C-2′), 123.31 (CH, C-7), 122.41 (C, C-5), 115.36 (CH, C-9), 105.71 (CH, C-3). MS: calcd for $C_{15}H_{10}N_2O_3$ m/z = 266, found 266.93. HPLC peak purity: 98.3%.

2-(4′-Nitro-phenyl)-1H-quinolin-4-one (3i). Pale yellow solid, yield (45%), m.p. 195–196 °C. ^{1}H NMR (DMSO-d_6, 600 MHz, 25 °C, TMS) δ ppm 11.56 (s, 1H, NH), 8.22–8.21 (d, 2H, H-3′, H-5′), 8.00 (d, 1H, H-6), 7.79–7.77 (d, 2H, H-2′, H-6′), 7.67 (d, 1H, H-9), 7.62–7.54 (t, t, 2H, H-7, H-8), 6.32 (s, 1H, H-3); ^{13}C NMR (DMSO-d_6, 150 MHz, 25 °C, TMS) δ ppm 182.44 (C═O, C-4), 151.79 (C, C-2), 151.79 (C, C-4′), 147.79 (C, C-1′), 142.32 (C, C-10), 141.66 (CH, C-8), 133.43 (CH, C-2′), 128.76 (CH, C-6′), 125.01 (CH, C-6), 124.31 (CH, C-3′), 124.21 (CH, C-5′), 123.31 (CH, C-7), 122.41 (C, C-5), 115.36 (CH, C-9), 105.65 (CH, C-3).

*4.2.2.4. General procedure for synthesis of cinnamic acid-piperazine hybrids (**4a** – **4e**).* Synthetic scheme is shown in Scheme 2. Substituted cinnamic acid (1 mol) was taken in organic solvent (dichloromethane, DCM) and thionyl chloride (1.2 mol) was added followed by addition of catalytic amount of dimethylformamide (DMF). The reaction mixture was refluxed for 24 h. Completion of reaction was monitored by TLC (Hexane:Ethyl acetate:methanol; 3:2:0.5). After completion of reaction, solvent was evaporated to remove excess of thionyl chloride and to get cinnamoyl chloride in the form of an amorphous powder. Unsubstituted piperazine (3 mol) was dissolved in DCM and triethylamine (TEA) (3 equivalent) was added to it and stirred at 0 °C. Substituted cinnamoyl chloride (1 mol) was dissolved in DCM and added dropwise to above stirred solution at 0 °C. Completion of reaction was monitored by TLC (Hexane : Ethyl acetate : methanol; 3:2:0.5). After completion, the precipitate obtained was filtered and washed with water. The resulting solid product was suspended in 5% sodium bicarbonate solution to remove any acid impurity. The final product was recrystallized from absolute alcohol.

3-Phenyl-1-piperazin-1-yl-propenone (4a). White solid, yield (61.85%), m.p. 264–265 °C. ^{1}H NMR ($CDCl_3$, 600 MHz, 25 °C, TMS) δ ppm 7.7 (d, 1H, H-7), 7.5 (d, 2H, H-2, H-6), 7.3 (m, 3H, H-3, H-4, H-5), 6.8 (d, 1H, H-8), 3.8 (bd, 6H, H-2′, H-3′, H-5′, H-6′), 1.6 (s, 1H, NH); ^{13}C NMR ($CDCl_3$ 200 MHz, 25 °C, TMS) δ ppm 165.74 (C═O, C-9), 143.7 (CH, C-7), 135 (C, C-1), 129.9 (CH, C-4), 128.8 (CH, C-3, C-5), 127.8 (CH, C-2, C-6), 116.40 (CH, C-8), 45.9 (CH_2, C-2′, C6′), 42.2 (CH_2, C-3′, C-5′). MS: calcd for $C_{13}H_{16}N_2O$ m/z = 216, found 216.99. HPLC peak purity: 93.2%.

3-(2-Methoxy-phenyl)-1-piperazin-1-yl-propenone (4b). White solid, yield (57%), m.p. 224–225 °C. ^{1}H NMR ($CDCl_3$, 600 MHz, 25 °C, TMS) δ ppm 7.94 (d, 1H, H-7), 7.5 (d, 1H, H-6), 7.33 (t, 1H, H-5), 6.96 (d, t, d, 3H, H-3, H-4, H-8), 3.8 (s, 1H, H-2), 3.7 (bd, 6H, H-2′, H-3′, H-5′, H-6′), 1.6 (s, 1H, NH); ^{13}C NMR ($CDCl_3$ 200 MHz, 25 °C, TMS) δ ppm 166.4 (C═O, C-9), 158.2 (C, C-2), 139.1 (CH, C-7), 130.9 (CH, C-4), 129.2 (CH, C-6), 124.0 (C, C-1), 120.6 (CH, C-5), 117.4 (CH, C-8), 111.1 (CH, C-3), 55.5 (OCH_3), 45.6 (CH_2, C-2′, C6′), 42.1 (CH_2, C-3′, C-5′). MS: calcd for $C_{14}H_{18}N_2O_2$ m/z = 246, found 246.16. HPLC peak purity: 99.8%.

3-(4-Methoxy-phenyl)-1-piperazin-1-yl-propenone (4c). White solid, yield (66%), m.p. 240–242 °C. ^{1}H NMR ($CDCl_3$, 600 MHz, 25 °C, TMS) δ ppm 7.6 (d, 1H, H-7), 7.4 (d, 2H, H-2, H-6), 6.9 (d, 2H, H-3, H-5), 6.7 (d, 1H, H-8), 3.8 (s, 1H, H-4), 3.7 (bd, 6H, H-2′, H-3′, H-5′, H-6′), 1.57 (s, 1H, NH); ^{13}C NMR ($CDCl_3$ 200 MHz, 25 °C, TMS) δ ppm 166.0 (C═O, C-9), 161.0 (C, C-4), 143.3 (CH, C-7), 129.4 (CH, C-2, C-6), 127.7 (C, C-1), 114.2 (CH, C-3, C-5), 113.8 (CH, C-8), 55.3 (OCH_3), 45.5 (CH_2, C-2′, C6′), 42.1 (CH_2, C-3′, C-5′). MS: calcd for $C_{14}H_{18}N_2O_2$ m/z = 246, found 246.17. HPLC peak purity: 99.9%.

3-(3,4-Dimethoxy-phenyl)-1-piperazin-1-yl-propenone (4d). White solid, yield (70%), m.p. 241–242 °C. ^{1}H NMR ($CDCl_3$, 600 MHz, 25 °C, TMS) δ ppm 7.6 (d, 1H, H-7), 7.1 (d, 1H, H-6), 7.0 (s, 1H, H-2), 6.8 (d, 1H, H-5), 6.7 (d, 1H, H-8), 3.93 (s, 1H, H-4), 3.91 (s,1H, H-3), 3.8 (bd, 6H, H-2′, H-3′, H-5′, H-6′), 1.58 (s, 1H, NH); ^{13}C NMR ($CDCl_3$ 200 MHz, 25 °C, TMS) δ ppm 165.9.0 (C═O, C-9), 150.8 (C, C-3), 149.1 (C, C-4), 143.7 (CH, C-7), 127.9 (C, C-1), 122.0 (CH, C-8), 114.0 (CH, C-6), 111.1 (CH, C-5), 109.9 (CH, C-2), 55.9 (OCH_3), 45.6 (CH_2, C-2′, C6′), 42.1 (CH_2, C-3′, C-5′). MS: calcd for $C_{15}H_{20}N_2O_3$ m/z = 276, found 276.28. HPLC peak purity: 99.9%.

3-(4-Chloro-phenyl)-1-piperazin-1-yl-propenone (4e). Off-white solid, yield (76%), m.p. 275–276 °C. ^{1}H NMR ($CDCl_3$, 600 MHz, 25 °C, TMS) δ ppm 7.6 (d, 1H, H-7), 7.4 (d, 2H, H-3, H-5), 7.3 (d, 2H, H-2, H-6), 6.8 (d, 1H, H-8), 3.76 (bd, 6H, H-2′, H-3′, H-5′, H-6′), 1.57 (s, 1H, NH).

4.2.3. In vitro evaluation

4.2.3.1. Cells and virus

4.2.3.1.1. Maintenance of MDCK cells. Madin-Darby canine kidney (MDCK) cells were grown in minimum essential medium (MEM, Gibco, by Life Technologies) complemented with 10% foetal bovine serum (FBS, Gibco, by Life Technologies) and 1% Antibiotic (10,000 U/mL penicillin and 0.5 mg/mL streptomycin) (Gibco, by Life Technologies).

4.2.3.1.2. Preparation of virus stock. The influenza A(H1N1)pdm09 virus was propagated in MDCK cells in the presence of 2 μg/mL tosyl phenylalanyl chloromethyl ketone (TPCK)-trypsin. The stock of virus was obtained by adding 500 μL of A(H1N1)pdm09 virus to 85–90% confluent MDCK cells after removing the medium from flask and incubated for 1 h at 37 °C with 5% CO_2 to maximize the viral adsorption to the cells. Subsequently, 4.5 mL of viral growth medium (2 μg/mL TPCK-trypsin + MEM) was added and incubated at above mentioned conditions for 5–7 days. Supernatant was then collected based on cytopathic effect of the virus and stored at −80 °C. These were repeated several times for adequate virus stock.

4.2.3.2. Cytotoxicity studies. Cytotoxicity studies of the synthesized molecules and standard drug *viz.* oseltamivir phosphate (OMVP) were carried out by MTT-Formazan assay [58]. MDCK cells were inoculated into 96-well plates and incubated at 37 °C with 5% CO_2 for 24 h until grown to 90% confluency. The media was then replaced with serum-free DMEM (Dulbecco's Modified Eagle Medium, without phenol red) containing serially diluted molecules (1000, 500, 250, 200, 125, 100, 40,

10, 1, 0.1 μM corresponding to 10-folds, 5-folds and 2-folds dilutions). After 16 h of incubation, the media was removed and 100 μL of a 0.5 mg/mL MTT (3-(4,5-Dimethylthiozol-2-yl)-3,5-dipheryl tetrazolium bromide, Sigma-Aldrich) solution was added to each well and incubated at 37 °C for 4 h. After removal of supernatant, 100 μL of dimethylsulfoxide (DMSO, Sigma-Aldrich) was added to each well so that the formed formazan crystals get dissolved. Absorbance was measured at 540 nm in a microplate reader. Data were normalized following the equation: Cell viability (%) = (sample value - blank control)/(cell control - blank control) × 100. The cytotoxic concentration 50% (CC_{50}) was calculated as the concentration at which 50% cells remain viable. It was calculated in GraphPad Prism 5 from a dose response curve obtained using a non-linear regression (curve fit).

4.2.3.3. Cytopathic effect (CPE) inhibition assay. The virus (100 μL) was inoculated onto near confluent MDCK cell monolayers for 1 h to allow for viral adsorption in 24-well plates after removing the media at 37 °C under 5% CO_2 atmosphere. 2 mL of molecules prepared at different concentrations (500, 250, 200, 125, 100, 10, 1, 0.1 μM) in MEM containing 2 μg/mL TPCK-trypsin was added in the allotted wells. The cultures were incubated for 3–4 days at 37 °C under 5% CO_2 atmosphere to develop CPE if any, checked every day. Controls were set consisting of only cells (i.e. no virus, no drug), referred as Cell Control (CC); and cells with virus only (i.e. virus but no drug), referred as Virus Control (VC). The candidate molecule was said to have antiviral activity if there was absence of viral CPE. The antiviral effect of the molecules was determined by grading system developed by Kudi and Myint mentioned in our previous work [59]. After 3–4 days, when VC showed 95–100% CPE, the supernatant from each well was removed and tested for hemagglutination (HA) titer of virus. The reduction of HA titer of virus in molecule treated wells was compared to HA titer of virus in VC well. The HA titer was determined by means of hemagglutination inhibition (HAI) assay.

4.2.3.4. Hemagglutination inhibition (HAI) assay. Serial two-fold dilutions of supernatant of infected cells (100 μL) were prepared using 1X PBS in a 96-well U-bottom plate. A 50 μL of 1% chicken red blood cells was added to each well. After 30 min incubation at 22 °C, hemagglutination (reddish mesh across entire well) and precipitation of red blood cells (red dot in the centre of well) was noted. The highest dilution factor that caused hemagglutination is the HA titer of the virus. [60]. HA titer of the VC and molecule treated wells was compared to ascertain the reduction in %HA viral titer treated by molecules.

4.2.3.5. Cell-based screening of hit molecules using crystal violet (CV) assay. CV assay was executed by reported method [61,62], with few modifications. MDCK cells were seeded in 48-well tissue culture plates and incubated for 24 h at 37 °C under 5% CO_2 atmosphere. The media was aspirated. Controls were set i.e., CC and VC (as discussed above) along with DC (Drug control i.e., only drugs and cells). 30 μL of virus dilution (256 HA units/mL) was added in each well except for CC and DC. The plates were incubated for 1 h for maximum adsorption of virus. The dilutions of candidate molecules at different concentrations (100 μM to 0.001 μM) were then added in the treatment cells while serum free media was added in CC, DC and VC. The plates were kept for incubation at 37 °C under 5% CO_2 atmosphere for 24–36 h till the CPE was observed. Further, the media was aspirated from all wells and washings were given twice with 1X PBS. Plates were inverted on filter paper and tapped to remove remaining fluid. 100 μL of crystal violet (0.5%) was added to each well and incubated for 20 min at room temperature (RT) on a bench rocker with frequency of 20 oscillations/min. The plates were washed with tap water to remove the unbound dye. Plates were inverted on filter paper and tapped to remove remaining fluid. The plates were air dried at RT without the lid on. 300 μL of absolute methanol was added to each well and incubated with lid on for 20 min at RT on bench rocker with a frequency of 20 oscillations/min. Optical density (OD) was measured at 570 nm. The percentage cell survival in wells treated with molecules was calculated in reference to the uninfected untreated control i.e., CC and plotted against the molecule's concentration. EC_{50} was calculated using a linear regression analysis tool. The experiment was performed in triplicate for each candidate molecule.

4.2.3.6. Enzyme-based NA inhibition assay. NA inhibitory activity was determined using the NA-*Star*® influenza neuraminidase inhibitor resistance detection kit (Applied Biosystem) as per previously reported method [13]. Succinctly, 25 μL of candidate molecules (conc. ranging from 100 μM to 0.001 μM) or quercetin (QR, conc. ranging from 100 μM to 0.001 μM) or oseltamivir carboxylate (OMVC, conc. ranging from 1000 nM to 1 nM) at two times the desired concentration was added in duplicate to a 96-well microtiter plate. H1N1 virus was diluted 5-fold with the assay buffer. To the plate, 25 μL of the diluted virus was mixed with the molecules and incubated at 37 °C for 20 min. The substrate was diluted at 1:1000 in assay buffer immediately before use. Then 10 μL of the diluted substrate were added to each well. The reaction mixtures were kept for incubation at RT for 15 min and then activated by adding 60 μL of accelerator. The chemiluminescent signal was quantified immediately by microplate reader [63]. A 50% inhibitory concentration (IC_{50}), relative to the activity in positive control i.e., the reaction mixture well containing virus but no test molecule, was determined to measure inhibitory activity of test molecules using GraphPad Prism 5.

4.2.3.7. Enzyme kinetics assay. The mechanism of NA inhibition was determined by kinetics assay with previously reported method [13]. To 96-well microtiter plate, 25 μL of OMVC or QR or candidate molecules (two conc. bracketing IC_{50}, along with I_0) was pre-incubated with 25 μL diluted H1N1 virus at 37 °C for 20 min. This was followed by addition of substrate (6.25, 12.5, 25, 50, 100 μM). Kinetic characterization for the hydrolysis of substrate catalysed by H1N1-NA was carried out by measuring the chemiluminescent signal of hydrolysis product. The parallel control experiment was implemented without molecules in the mixture. K_m and V_{max} values were obtained from GraphPad Prism 5.

4.2.4. Statistical analyses

Mean ± standard deviation (std dev, SD) of at least three independent biological replicates ($n \geq 3$) was considered for analyses. For antiviral assays, $p < 0.05$ (Mann-Whitney *U* test and Student's *t* test) was believed to be statistically significant. All the statistical analyses were performed using GraphPad Prism 5 and the R statistical environment.

Funding sources

The biological evaluation was funded by Indian Council of Medical Research (ICMR), New Delhi, India (58/36/2013-BMS).

Declaration of Competing Interest

The authors declare that they have no known competing financial interests or personal relationships that could have appeared to influence the work reported in this paper.

Acknowledgements

K. Malbari and M. Kanyalkar are grateful to ICMR (58/27/2007-BMS) for funding computational facility at Department of Pharmaceutical Chemistry, Prin K M Kundnani College of Pharmacy. K. Malbari is indebted to ICMR for Senior Research Fellowship (58/36/2013-BMS) and acknowledges Schrödinger Inc. for the trial license with OPLS3e forcefield. Authors also acknowledge the infrastructure funding provided by Department of Science and Technology's Fund for

Improvement of S&T Infrastructure in Higher Educational Institutions (DST-FIST), New Delhi (SR/FST/College-264/2015(C)) at Prin KM Kundnani College of Pharmacy, Mumbai, India. K. Malbari and M. Joshi acknowledge National NMR Facility provided by Tata Institute of Fundamental Research (TIFR), Colaba, Mumbai, India.

Appendix A. Supplementary material

Supplementary data to this article can be found online at https://doi.org/10.1016/j.bioorg.2021.105139.

References

[1] S.A. Bergervoet, C.K.Y. Ho, R. Heutink, A. Bossers, N. Beerens, Spread of Highly Pathogenic Avian Influenza (HPAI) H5N5 viruses in Europe in 2016–2017 appears related to the timing of reassortment events, Viruses 11 (2019) 501, https://doi.org/10.3390/v11060501.

[2] N.A. Gerloff, S.U. Khan, A. Balish, I.S. Shanta, N. Simpson, L. Berman, N. Haider, M.K. Poh, A. Islam, E. Gurley, M.A. Hasnat, T. Dey, B. Shu, S. Emery, S. Lindstrom, A. Haque, A. Klimov, J. Villanueva, M. Rahman, E. Azziz-Baumgartner, M. Ziaur Rahman, S.P. Luby, N. Zeidner, R.O. Donis, K. Sturm-Ramirez, C.T. Davis, Multiple reassortment events among highly pathogenic avian influenza A(H5N1) viruses detected in Bangladesh, Virology. 450–451 (2014) 297–307, https://doi.org/10.1016/j.virol.2013.12.023.

[3] K. Shanmuganatham, M.M. Feeroz, L. Jones-Engel, D. Walker, Smr. Alam, Mk. Hasan, P. McKenzie, S. Krauss, R.J. Webby, R.G. Webster, Genesis of avian influenza H9N2 in Bangladesh, Emerg. Microbes Infect. 3 (2014) e88–e88. DOI: 10.1038/emi.2014.84.

[4] C. Liu, M.C. Eichelberger, R.W. Compans, G.M. Air, Influenza type A virus neuraminidase does not play a role in viral entry, replication, assembly, or budding, J. Virol. 69 (1995) 1099–1106.

[5] Z.-M. Sheng, D.S. Chertow, X. Ambroggio, S. McCall, R.M. Przygodzki, R. E. Cunningham, O.A. Maximova, J.C. Kash, D.M. Morens, J.K. Taubenberger, Autopsy series of 68 cases dying before and during the 1918 influenza pandemic peak, Proc. Natl. Acad. Sci. U. S. A. 108 (2011) 16416–16421, https://doi.org/10.1073/pnas.1111179108.

[6] N.M. Bouvier, A.C. Lowen, Animal Models for Influenza Virus Pathogenesis and Transmission, Viruses. 2 (2010) 1530–1563, https://doi.org/10.3390/v20801530.

[7] J.K. Taubenberger, D.M. Morens, Influenza: the mother of all pandemics, Emerg. Infect. Dis. 12 (2006) (1918) 15–22, https://doi.org/10.3201/eid1201.050979.

[8] C.U. Kim, X. Chen, D.B. Mendel, Neuraminidase inhibitors as anti-influenza virus agents, Antivir. Chem. Chemother. 10 (1999) 141–154, https://doi.org/10.1177/095632029901000401.

[9] H.-L. Yen, E. Hoffmann, G. Taylor, C. Scholtissek, A.S. Monto, R.G. Webster, E. A. Govorkova, Importance of neuraminidase active-site residues to the neuraminidase inhibitor resistance of influenza viruses, J. Virol. 80 (2006) 8787–8795, https://doi.org/10.1128/JVI.00477-06.

[10] Y. Xie, D. Xu, B. Huang, X. Ma, W. Qi, F. Shi, X. Liu, Y. Zhang, W. Xu, Discovery of N-substituted oseltamivir derivatives as potent and selective inhibitors of H5N1 influenza neuraminidase, J. Med. Chem. 57 (2014) 8445–8458, https://doi.org/10.1021/jm500892k.

[11] E. Feng, W.-J. Shin, X. Zhu, J. Li, D. Ye, J. Wang, M. Zheng, J.-P. Zuo, K.T. No, X. Liu, W. Zhu, W. Tang, B.-L. Seong, H. Jiang, H. Liu, Structure-based design and synthesis of C-1- and C-4-modified analogs of zanamivir as neuraminidase inhibitors, J. Med. Chem. 56 (2013) 671–684, https://doi.org/10.1021/jm3009713.

[12] A.S. Chintakrindi, E.A.F. Martis, D.J. Gohil, S.T. Kothari, A.S. Chowdhary, E. C. Coutinho, M.A. Kanyalkar, A computational model for docking of noncompetitive neuraminidase inhibitors and probing their binding interactions with neuraminidase of influenza virus H5N1, Curr. Comput. Aided. Drug Des. 12 (2016) 272–281.

[13] A.S. Chintakrindi, D.J. Gohil, S.T. Kothari, A.S. Chowdhary, M.A. Kanyalkar, Design, synthesis and evaluation of chalcones as H1N1 Neuraminidase inhibitors, Med. Chem. Res. 27 (2018) 1013–1025, https://doi.org/10.1007/s00044-017-2124-2.

[14] K.D. Malbari, A.S. Chintakrindi, L.R. Ganji, D.J. Gohil, S.T. Kothari, M.V. Joshi, M. A. Kanyalkar, Structure-aided drug development of potential neuraminidase inhibitors against pandemic H1N1 exploring alternate binding mechanism, Mol. Divers. (2019), https://doi.org/10.1007/s11030-019-09919-6.

[15] K.M.P. Suruse, K. Malbari, A. Chintakrindi, D. Gohil, S. Srivastava, S. Kothari, A. Chowdhary, Virucidal activity of newly synthesized chalcone derivatives against H1N1 virus supported by molecular docking and membrane interaction studies, J. Antivir. Antiretrovir. 8 (2016) 79–89. DOI: 10.4172/jaa.1000139.

[16] T.T. Dao, P.H. Nguyen, H.S. Lee, E. Kim, J. Park, S. Il Lim, W.K. Oh, Chalcones as novel influenza A (H1N1) neuraminidase inhibitors from Glycyrrhiza inflata, Bioorg. Med. Chem. Lett. 21 (2011) 294–298, https://doi.org/10.1016/j.bmcl.2010.11.016.

[17] T.-T. Dao, B.-T. Tung, P.-H. Nguyen, P.-T. Thuong, S.-S. Yoo, E.-H. Kim, S.-K. Kim, W.-K. Oh, C-Methylated Flavonoids from Cleistocalyx operculatus and Their Inhibitory Effects on Novel Influenza A (H1N1) Neuraminidase, J. Nat. Prod. 73 (2010) 1636–1642, https://doi.org/10.1021/np1002753.

[18] Y.B. Ryu, J.H. Kim, S.-J. Park, J.S. Chang, M.-C. Rho, K.-H. Bae, K.H. Park, W. S. Lee, Inhibition of neuraminidase activity by polyphenol compounds isolated from the roots of Glycyrrhiza uralensis, Bioorg. Med. Chem. Lett. 20 (2010) 971–974, https://doi.org/10.1016/j.bmcl.2009.12.106.

[19] T.N.A. Nguyen, T.T. Dao, B.T. Tung, H. Choi, E. Kim, J. Park, S.I. Lim, W.K. Oh, Influenza A (H1N1) neuraminidase inhibitors from Vitis amurensis., Food Chem. 124 (2010) 437–443. doi: 10.1016/j.foodchem.2010.06.049.

[20] G. Patrick, Drug design: optimizing target interactions, in: G. Patrick, An Introd. to Med. Chem. Oxford, Oxford Univ. Press, 2013: pp. 215–247.

[21] H.D. Gravina, N.F. Tafuri, A. Silva Júnior, J.L.R. Fietto, T.T. Oliveira, M.A.N. Diaz, M.R. Almeida, In vitro assessment of the antiviral potential of trans-cinnamic acid, quercetin and morin against equid herpesvirus 1, Res. Vet. Sci. 91 (2011) e158–e162, https://doi.org/10.1016/j.rvsc.2010.11.010.

[22] A.P. Stankyavichyus, L.M.M. Stankyavichene, M.S. Sapragonene, L. V. Korobchenko, E.I. Boreko, G.V. Vladyko, Synthesis and antiviral activity of cinnamic acid derivatives, Pharm. Chem. J. 22 (1988) 896–900, https://doi.org/10.1007/BF00771641.

[23] R. Amano, A. Yamashita, H. Kasai, T. Hori, S. Miyasato, S. Saito, H. Yokoe, K. Takahashi, T. Tanaka, T. Otoguro, S. Maekawa, N. Enomoto, M. Tsubuki, K. Moriishi, Cinnamic acid derivatives inhibit hepatitis C virus replication via the induction of oxidative stress, Antiviral Res. 145 (2017) 123–130, https://doi.org/10.1016/j.antiviral.2017.07.018.

[24] R.J. Martin, Modes of action of anthelmintic drugs, Vet. J. 154 (1997) 11–34, https://doi.org/10.1016/S1090-0233(05)80005-X.

[25] WHO, Helminths: Intestinal nematode infection: Piperazine; WHO Model Prescribing Information: Drugs Used in Parasitic Diseases, 2nd ed., n.d.

[26] C. Viegas-Junior, A. Danuello, V. da Silva Bolzani, E.J. Barreiro, C.A.M. Fraga, Molecular hybridization: a useful tool in the design of new drug prototypes, Curr. Med. Chem. 14 (2007) 1829–1852, https://doi.org/10.2174/092986707781058805.

[27] M. Domenech de Celles, J.-S. Casalegno, B. Lina, L. Opatowski, Influenza may facilitate the spread of SARS-CoV-2, MedRxiv. (2020) 2020.09.07.20189779. DOI: 10.1101/2020.09.07.20189779.

[28] J.L. McAuley, B.P. Gilbertson, S. Trifkovic, L.E. Brown, J.L. McKimm-Breschkin, Influenza virus neuraminidase structure and functions, Front. Microbiol. 10 (2019) 26–32, https://doi.org/10.3389/fmicb.2019.00039.

[29] M. von Itzstein, R. Thomson, Anti-influenza drugs: the development of sialidase inhibitors BT - antiviral strategies, in: H.-G. Kräusslich, R. Bartenschlager (Eds.), Springer Berlin Heidelberg, Berlin, Heidelberg, 2009: pp. 111–154. DOI: 10.1007/978-3-540-79086-0_5.

[30] A. Chintakrindi, C.D. and M. Kanyalkar,, Rational development of neuraminidase inhibitor as novel anti-flu drug, Mini-Reviews, Med. Chem. 12 (2012) 1273–1281, https://doi.org/10.2174/138955712802761997.

[31] Q. Li, J. Qi, W. Zhang, C.J. Vavricka, Y. Shi, J. Wei, E. Feng, J. Shen, J. Chen, D. Liu, J. He, J. Yan, H. Liu, H. Jiang, M. Teng, X. Li, G.F. Gao, The 2009 pandemic H1N1 neuraminidase N1 lacks the 150-cavity in its active site, Nat. Struct. &Amp; Mol. Biol. 17 (2010) 1266. https://doi.org/10.1038/nsmb.1909.

[32] C.J. Vavricka, Q. Li, Y. Wu, J. Qi, M. Wang, Y. Liu, F. Gao, J. Liu, E. Feng, J. He, J. Wang, H. Liu, H. Jiang, G.F. Gao, Structural and functional analysis of laninamivir and its octanoate prodrug reveals group specific mechanisms for influenza NA inhibition, PLoS Pathog. 7 (2011), e1002249, https://doi.org/10.1371/journal.ppat.1002249.

[33] X. Xu, X. Zhu, R.A. Dwek, J. Stevens, I.A. Wilson, Structural characterization of the 1918 influenza virus H1N1 neuraminidase, J. Virol. 82 (2008) 10493–10501. DOI: 10.1128/JVI.00959-08.

[34] M.C. Zambon, The pathogenesis of influenza in humans, Rev. Med. Virol. 11 (2001) 227–241, https://doi.org/10.1002/rmv.319.

[35] I. Tubert-Brohman, W. Sherman, M. Repasky, T. Beuming, Improved Docking of Polypeptides with Glide, J. Chem. Inf. Model. 53 (2013) 1689–1699, https://doi.org/10.1021/ci400128m.

[36] T.A. Halgren, Identifying and characterizing binding sites and assessing druggability, J. Chem. Inf. Model. 49 (2009) 377–389.

[37] H.J. Jeong, Y.B. Ryu, S.J. Park, J.H. Kim, H.J. Kwon, J.H. Kim, K.H. Park, M. C. Rho, W.S. Lee, Neuraminidase inhibitory activities of flavonols isolated from Rhodiola rosea roots and their in vitro anti-influenza viral activities, Bioorganic Med. Chem. 17 (2009) 6816–6823, https://doi.org/10.1016/j.bmc.2009.08.036.

[38] M.R. Lentz, R.G. Webster, G.M. Air, Site-directed mutation of the active site of influenza neuraminidase and implications for the catalytic mechanism, Biochemistry. 26 (1987) 5351–5358, https://doi.org/10.1021/bi00391a020.

[39] C. D'Souza, M. Kanyalkar, M. Joshi, E. Coutinho, S. Srivastava, Search for novel neuraminidase inhibitors: Design, synthesis and interaction of oseltamivir derivatives with model membrane using docking, NMR and DSC methods, Biochim. Biophys. Acta - Biomembr. 1788 (2009) 1740–1751, https://doi.org/10.1016/j.bbamem.2009.04.014.

[40] M.P. Gleeson, A. Hersey, S. Hannongbua, In-silico ADME models: a general assessment of their utility in drug discovery applications, Curr. Top. Med. Chem. 11 (2011) 358–381.

[41] W.J. Dunn, M.G. Koehler, S. Grigoras, The role of solvent-accessible surface area in determining partition coefficients, J. Med. Chem. 30 (1987) 1121–1126, https://doi.org/10.1021/jm00390a002.

[42] W. Chu, D. Zhou, V. Gaba, J. Liu, S. Li, X. Peng, J. Xu, D. Dhavale, D.P. Bagchi, A. d'Avignon, N.B. Shakerdge, B.J. Bacskai, Z. Tu, P.T. Kotzbauer, R.H. Mach, Design, synthesis, and characterization of 3-(benzylidene)indolin-2-one derivatives as ligands for α-synuclein fibrils, J. Med. Chem. 58 (2015) 6002–6017, https://doi.org/10.1021/acs.jmedchem.5b00571.

[43] L. Sun, N. Tran, F. Tang, H. App, P. Hirth, G. McMahon, C. Tang, Synthesis and biological evaluations of 3-substituted indolin-2-ones: A novel class of tyrosine kinase inhibitors that exhibit selectivity toward particular receptor tyrosine kinases, J. Med. Chem. 41 (1998) 2588–2603, https://doi.org/10.1021/jm980123i.
[44] A. Andreani, M. Rambaldi, A. Locatelli, A. Bongini, R. Bossa, I. Galatulas, M. Ninci, Synthesis and cardiotonic activity of pyridylmethylene-2-indolinones, Eur. J. Med. Chem. 27 (1992) 167–170.
[45] C. Klöck, X. Jin, K. Choi, C. Khosla, P.B. Madrid, A. Spencer, B.C. Raimundo, P. Boardman, G. Lanza, J.H. Griffin, Acylideneoxoindoles: a new class of reversible inhibitors of human transglutaminase 2, Bioorg. Med. Chem. Lett. 21 (2011) 2692–2696, https://doi.org/10.1016/j.bmcl.2010.12.037.
[46] A. Pelter, R.S. Ward, H.G. Heller, Carbon-13 nuclear magnetic resonance spectra of (Z)-and (E)-aurones, J. Chem. Soc. Perkin Trans. 1 (1979) 328–329.
[47] B.E. Davies, Pharmacokinetics of oseltamivir: an oral antiviral for the treatment and prophylaxis of influenza in diverse populations, J. Antimicrob. Chemother. 65 Suppl 2 (2010) ii5–ii10. DOI: 10.1093/jac/dkq015.
[48] P.C. Wagaman, H.A. Spence, R.J. O'Callaghan, Detection of influenza C virus by using an in situ esterase assay, J. Clin. Microbiol. 27 (1989) 832–836, https://pubmed.ncbi.nlm.nih.gov/2745694.
[49] G.M. Sastry, M. Adzhigirey, T. Day, R. Annabhimoju, W. Sherman, Protein and ligand preparation: parameters, protocols, and influence on virtual screening enrichments, J. Comput. Aided. Mol. Des. 27 (2013) 221–234, https://doi.org/10.1007/s10822-013-9644-8.
[50] A. Gaymard, N. Le Briand, E. Frobert, B. Lina, V. Escuret, Functional balance between neuraminidase and haemagglutinin in influenza viruses, Clin. Microbiol. Infect. 22 (2016) 975–983, https://doi.org/10.1016/j.cmi.2016.07.007.
[51] J.N. Varghese, P.M. Colman, Three-dimensional structure of the neuraminidase of influenza virus A/Tokyo/3/67 at 2.2 A resolution, J. Mol. Biol. 221 (1991) 473–486. DOI: 10.1016/0022-2836(91)80068-6.
[52] T. Halgren, New method for fast and accurate binding-site identification and analysis, Chem. Biol. Drug Des. 69 (2007) 146–148, https://doi.org/10.1111/j.1747-0285.2007.00483.x.
[53] LigPrep, Schrödinger, LLC, New York, NY, 2019, (n.d.).
[54] R.A. Friesner, J.L. Banks, R.B. Murphy, T.A. Halgren, J.J. Klicic, D.T. Mainz, P. S. Shenkin, Glide,, A new approach for rapid, accurate docking and scoring. 1. Method and assessment of docking accuracy, J. Med. Chem. (2004).
[55] W. Sherman, T. Day, M.P. Jacobson, R.A. Friesner, R. Farid, Novel procedure for modeling ligand/receptor induced fit effects, J. Med. Chem. 49 (2006) 534–553.
[56] QikProp, Schrödinger, LLC, New York, NY, 2019, (n.d.).
[57] R. Abonia, P. Cuervo, J. Castillo, B. Insuasty, J. Quiroga, M. Nogueras, J. Cobo, Unexpected intramolecular cyclization of some 2′-aminochalcones to indolin-3-ones mediated by Amberlyst®-15, Tetrahedron Lett. 49 (2008) 5028–5031.
[58] T. Mosmann, Rapid colorimetric assay for cellular growth and survival: application to proliferation and cytotoxicity assays, J. Immunol. Methods. 65 (1983) 55–63.
[59] A.C. Kudi, S.H. Myint, Antiviral activity of some Nigerian medicinal plant extracts, J. Ethnopharmacol. 68 (1999) 289–294.
[60] S.M. Hosseini, E. Amini, M. Tavassoti Kheiri, P. Mehrbod, M. Shahidi, E. Zabihi, Anti-influenza Activity of a Novel Polyoxometalate Derivative (POM-4960), Int. J. Mol. Cell. Med. 1 (2012) 21–29, https://www.ncbi.nlm.nih.gov/pubmed/24551755.
[61] M. Feoktistova, P. Geserick, M. Leverkus, Crystal violet assay for determining viability of cultured cells, Cold Spring Harb. Protoc. 2016 (2016) pdb.prot087379. DOI: 10.1101/pdb.prot087379.
[62] J.N. Makau, K. Watanabe, T. Ishikawa, S. Mizuta, T. Hamada, N. Kobayashi, Identification of small molecule inhibitors for influenza a virus using in silico and in vitro approaches, PLoS One. 12 (2017) e0173582.
[63] J. An, D.C.W. Lee, A.H.Y. Law, C.L.H. Yang, L.L.M. Poon, A.S.Y. Lau, S.J.M. Jones, A novel small-molecule inhibitor of the avian influenza H5N1 virus determined through computational screening against the neuraminidase, J. Med. Chem. 52 (2009) 2667–2672, https://doi.org/10.1021/jm800455g.